Chapter 2

Biochar from *Citrullus Lanatus*: Preparation, Characterization, and Adsorptive Potential

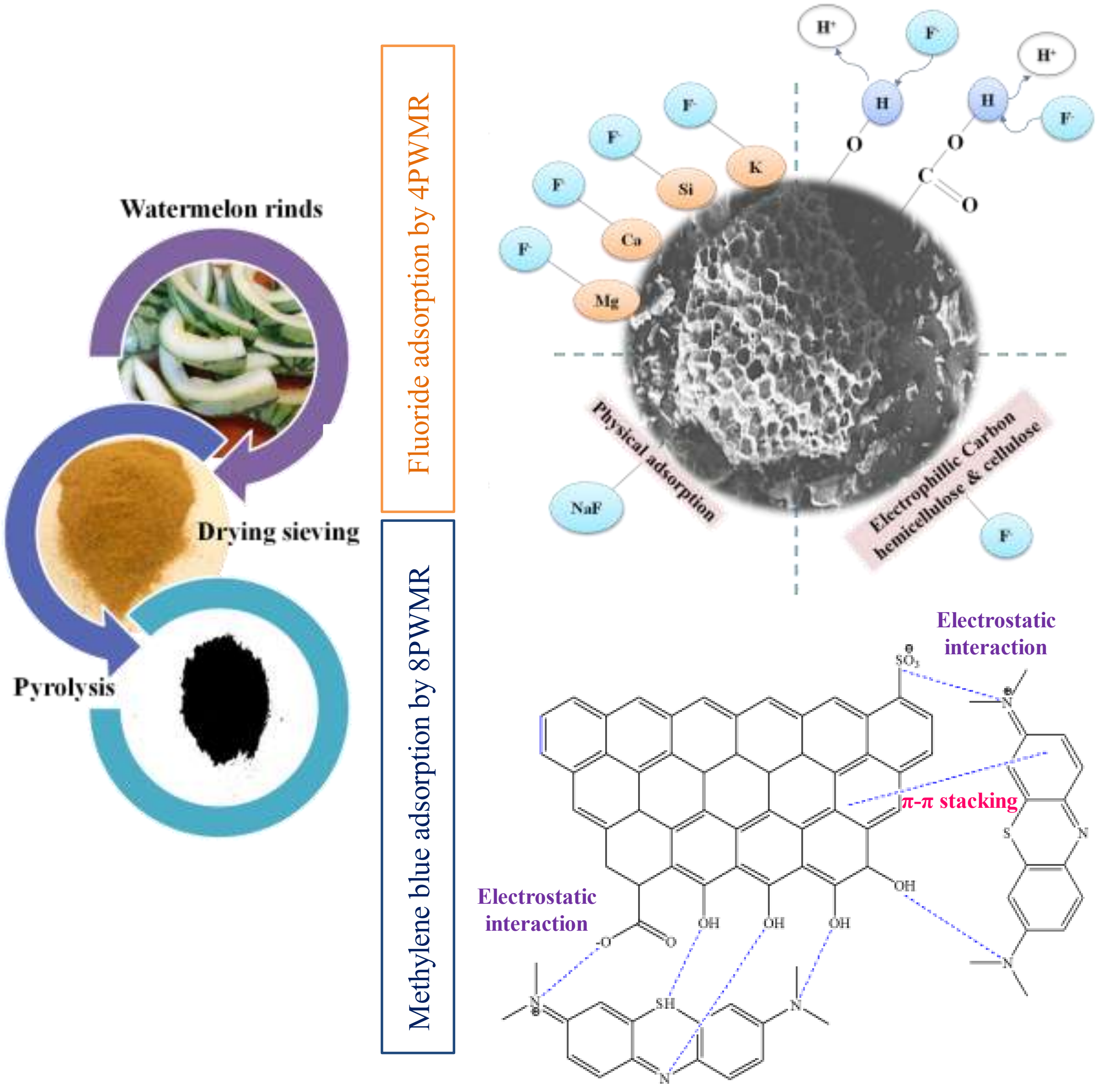

2.1 Introduction

Adsorption is one of the techniques that has been widely employed as a low-cost and highly effective fluoride removal approach (Bhatnagar et al., 2011). Biochar has been attracting attention as a green, sustainable and cost-effective adsorbent. The constituent content, chemical structure and stability of biochar are all considerably impacted by the characteristics of the raw feedstock biomass and pyrolysis conditions, particularly the temperature (Mohan et al., 2014). Specific features are imparted to the final biochar, such as ash content, its elemental composition, density and hardness (Mohan et al., 2014)(Brewer et al., 2009). Biochar has been used to remove herbicides (Wang et al., 2010), pesticides (Yang et al., 2010), fungicides (Yang et al., 2010) and metal ions (Zhao et al., 2019).

There has been very little research into the use of biochar for fluoride removal. Mohan et al. used magnetic and nonmagnetic biochars from corn stover (Mohan et al., 2014) as well as pine wood and pine bark chars (N. et al., 2012) to remove fluoride at pH 2. Goswami et al. developed nano-sized rice husk biochar (Tarazona-Díaz et al., 2011) for fluoride removal. However, in these studies, biochar was used to remove fluoride from ground water. Further, bio adsorbents such as banana peel, groundnut shell and perennial grass have been used to treat fluoride containing industrial wastewater (Petkowicz et al., 2016)(X. Jin et al., 2011b).

The features of the raw feedstock biomass, such as ash concentration and elemental components, density and hardness, impart certain properties to the resultant biochar. In particular, biochar from grass, corn stover and manure feedstocks has a higher ash content than biochar from other sources (Sadhu et al., 2022), while biochar made from straw has a lower specific surface area and microbiological stability than biochar made from wood. In last decade many activated carbons have been prepared from agro-industrial waste biomasses such as cashew nut shell (P. S. Kumar et al., 2011), tea (*Camellia sinensis* L.) seed shells (Gao et al., 2013), vetiver roots (Altenor et al., 2009), peach stones (Attia et al., 2008), cotton stalk (Deng et al., 2009), date stones (Foo & Hameed, 2011), pea shells (Geçgel et al., 2013) and banana stem (Misran et al., 2018)**.**

Citrullus lanatus (Watermelon) is a commercially important fruit in the Cucurbitaceae family. Watermelon is one of the most abundant fruits in India because of its tropical nature. Its production occupies 6–7% of overall fruit production in summer. Its global production was estimated to be around 93,700 million tonnes (Budrat & Shotipruk, 2009). Watermelon rind (WMR) is used in pickles and preserves, as well as for pectin extraction, and watermelon seeds are a potential source of protein (Horax et al., 2005). The rind is one of the major solid wastes produced by several Indian restaurants and cottage food industries.

WMR contains a fair amount of carbohydrates, phenolic compounds and fatty acids. The carbohydrate fraction of melon rind is primarily composed of cellulose, hemicelluloses and pectin, with the major monosaccharides being glucose, xylose and galactose, making WMR a potential candidate for biochar fabrication (Wu et al., 2012). Prakash Maran et al. extracted pectin by microwave-assisted extraction (MAE) from waste *Citrullus lanatus* fruit rind (X. Jin et al., 2011a). Lucas- Torres et. al. used montmorillonite clay in sugar dehydration processes from cellulose and hemicellulose fractions of melon rind waste to get competitive yields of 5-HMF and levulinic acid obtained which are useful in the biofuel industry (Bokhari et al., 2016). Odewunmi et al. extracted l-Citrulline from watermelon rind extract and used it as active corrosion inhibitor for mild steel in acidic medium (Odewunmi et al., 2015)**.**

The main objective of the work presented in this chapter was to synthesize biochar at different temperature from locally derived watermelon rind (WMR) and to evaluate the adsorption performance of biochar for the removal of fluoride and methylene blue (MB). The adsorption equilibrium and kinetics were determined. The effect of solution pH, adsorbent dose, contact time and temperature on the adsorption process was examined.

The physicochemical properties of pyrolyzed watermelon rind (PWMR) were determined and the efficiency of fluoride and methylene blue (MB) were investigated using batch adsorption as a function of pH, contact time, adsorbent dose and temperature. The biochar's performance was assessed using the Langmuir, Freundlich, Temkin and Halsey adsorption models. The thermodynamics and kinetics of the adsorption process was also investigated to gain a better understanding of the adsorption mechanism and the adsorption capacity of PWMR was compared to previously reported adsorbents for fluoride removal.

2.2 Materials and Methods

2.2.1 Synthesis of watermelon rind biochars

The watermelon rind waste was collected from the local fruit shop of Vadodara, Gujarat, India. The collected waste was washed thoroughly with water to remove dirt and dried in an oven at 100^{o}C for 24 h and then ground to get fine powder. This powder was then passed through 18 mesh sieve and stored in airtight polypropylene container. The sieved powder was pyrolyzed in a muffle furnace at 400 ^{o}C, 600 ^{o}C, 800 ^{o}C (at a rate of 10 ^{o}C/minute) for 1 h. The resulting biochar was washed with hot water before being dried in an oven at 100 ^{o}C (named 4PWMR, 6PWMR, 8PWMR respectively).

2.2.2 Characterization of the adsorbent

The adsorbent was characterized for its physiochemical properties using conventional chemical and analytical techniques.

Zeta potential Analysis

Charge Measurement was done by Zeta sizer ZetaPlus 90Plus/BI-MAS Brook Haven model.

Thermogravimetric analysis (TGA)

Thermo gravimetric analysis is an analytical technique used to determine a material's thermal stability and its fraction of volatile components by monitoring the weight change that occurs as a specimen is heated. Thermo gravimetric analysis was done using EXSTAR6000 TG/DTA 6300 model instrument. The measurements were done in nitrogen atmosphere. In the sample pan, sample weighing 5-10 mg was placed, and the temperature was raised from 30 to 500°C at a rate of 10 °C per minute. The mass of the sample pan was measured continuously as a function of temperature.

DSC analysis

DSC measurements were done on a DSC Q10 model (make TA Instruments). The samples were heated at a rate of 10 °C / min from 25 to 400 °C under a nitrogen atmosphere.

X-ray Diffraction (XRD) Analysis

XRD measurements of the powder samples were performed with a PANalytical Diffractometer (Bruker) using Cu-Kα radiation (λ=0.15418 nm) at a voltage of 45 kV and a scanning range of 2θ 0°-80°.

FT-IR spectra

The FT-IR spectral data were obtained at wavelengths ranging from 400-4000 cm^{-1}, using Spectrum II Perkin Elmer Fourier Transform Infrared Spectrophotometer in transmittance mode.

Scanning Electron Microscopy and Energy Dispersive X-ray Analysis

Scanning Electron Microscopy (SEM) was performed on TM3000 make Hitachi microscope to observe the surface morphology of biochars and after adsorption. The accelerating voltage was 10-20keV.

EDS analysis was done using a SEM/EDX (JEOL, model JSM-5610LV) microscope operating at 200 kV for obtaining the elemental composition of the biochars under study. The intensity or area of a peak in an EDAX spectrum is proportional to the concentration of the corresponding element in the specimen. For determining elemental content, the electron-beam current was assumed to be uniform throughout the specimen and electron channelling was avoided by avoiding strong diffraction conditions.

2.3 Results and Discussion

2.3.1 Characterisation of biochars

Thermogravimetric analysis

The 4PWMR adsorbent's thermogram is displayed in figure 2.1(a). The first stage weight loss (20%) from 50° to 100°C was attributed to the loss of moisture. Due to the evaporation of volatile substances and the breakdown of cellulose, hemicellulose and lignin components between 265°C and 500°C, the mass of biochar fell by 85%. A larger volatile matter content in the biochar was suggested by the significant weight reduction. Hemicellulose is said to thermally degrade around 250 °C and continue up to 380 °C, cellulose breaks down between 300 °C and 400 °C and lignin breaks down between 200 °C and 500 °C (Mimmo et al., 2014). There was no appreciable weight loss between 500 and 700 °C, the 11 % residual together with crystals including quartz, calcite, sylvite and whitlockite served as a marker of the fixed carbon content.

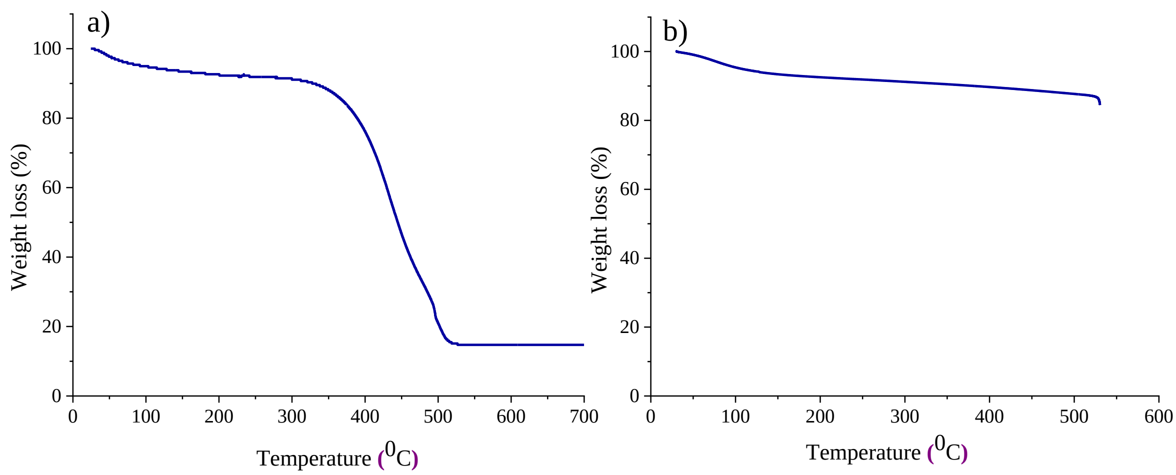

Figure 2.1 Thermogravimetric analysis of a) 4PWMR, b) 8PWMR

Figure 2.1(b) shows the thermogravimetric analysis (TGA) of 8PWMR. The thermogram exhibited 2 stages of weight loss. The first stage weight loss (~6.4%) from 50°-150°C may be ascribed to the loss of water. Between 265°C to 500°C, the biochar exhibited ~ 4.6 % weight loss that may be attributed to decomposition of unpyrolysed lignocellulosic fraction and other volatile fractions (Cabeza et al., 2015). The final mass of the biochar was about ~ 89.1% of its initial mass suggesting the presence of high mineral content.

DSC analysis

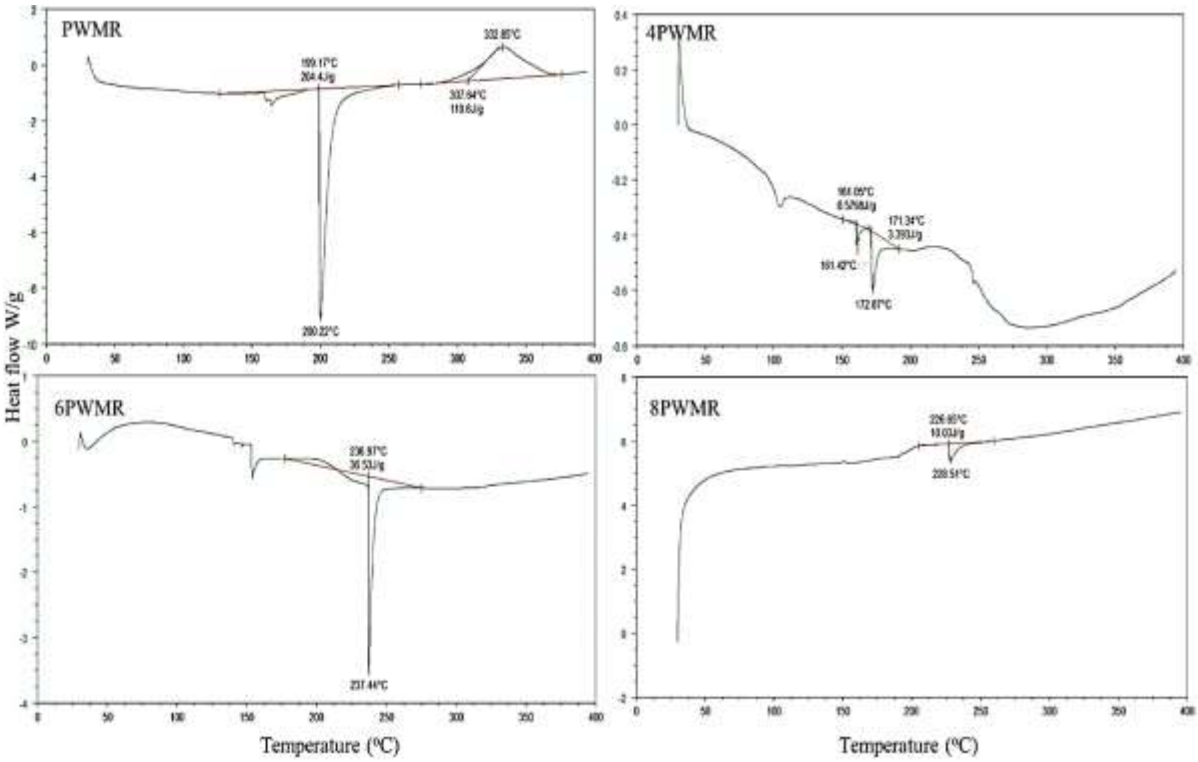

Figure 2.2 DSC analysis of biochars

The DSC thermogram of biochars is shown in figure 2.2. The endothermic peak observed in WMR at 200.22 ^{o}C may be attributed to loss of water molecules held by adsorption/adhesion to hemicellulose while exothermic peak at 332.85 ^{o}C may be attributed to break down and decomposition of cellulose, hemicellulose and lignin. The three endothermic peaks in 4PWMR at 100 ^{o}C, 161 ^{o}C and 172 ^{o}C may be attributed to evaporation of absorbed water from hemicellulose, cellulose and lignin. Two endothermic peaks at 150 ^{o}C and 237 ^{o}C in 6PWMR may be attributed to loss of water and pyrolysis of hemicellulose respectively. On the other hand, in 8PWMR the endothermic peak at 228.5 ^{o}C may be attributed to pyrolysis of hemicellulose and partial pyrolysis of cellulose.

XRD analysis

The peaks typical of cellulose were most prominent in the XRD spectrum of WMR (figure 2.3) while the weak broad peak observed at 2θ=44° corresponded to the graphitic (100) crystalline lattice of turbostratic carbon (i.e. there is very little or no stacking order between small graphene planes) in 4PWMR after fluoride adsorption. The Scherrer equation determined that the average crystallite size was 38 nm.

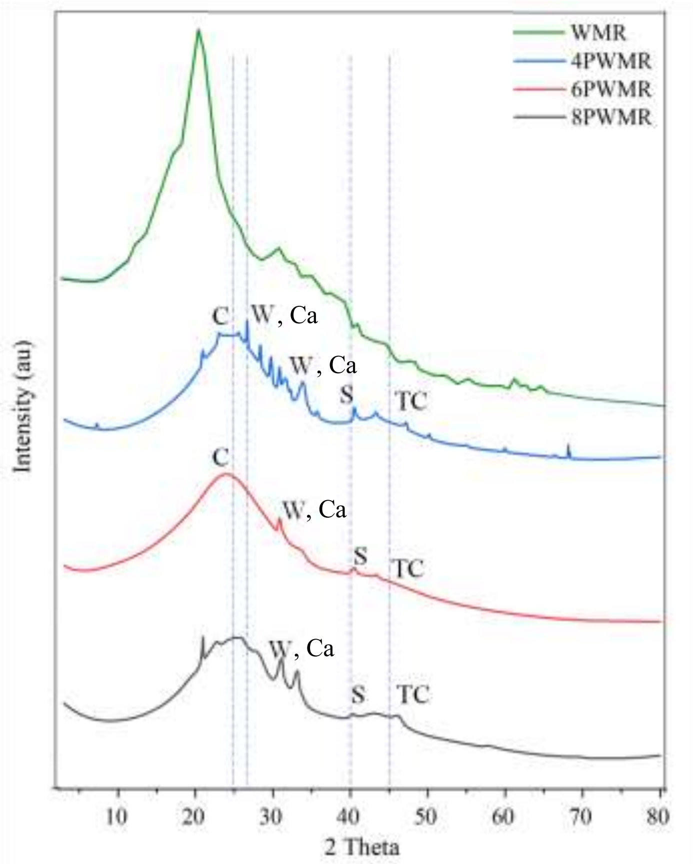

Figure 2. 3 XRD spectra of WMR, 4PWMR, 6PWMR and 8PWMR

The phase purity and crystallinity of the pure dried watermelon rind and pyrolyzed WMR at different temperature were examined by X-ray diffraction technique (XRD). The XRD pattern of the WMR was also shown for comparison (figure 2.3). The XRD spectra of WMR exhibited predominantly the peak characteristic of cellulose. The disappearance of peaks in 4PWMR, 6PWMR and 8PWMR indicated the decomposition of cellulose. The broad peak at ~2θ=22.8º can be indexed to the carbon (002) diffraction plane. Several other researchers (Dari et al., 2016)(Cabeza et al., 2015) have noticed these tiny graphene planes grouped in turbostratic disarray. The peaks at near 25.5º in 4PWMR, 6PWMR and 8PWMR are indicate the graphitic carbon (Li et al., 2009).

Additionally, other sharp peaks seen in 4PWMR at 28.5 and 40.6 were attributed to quartz (q) and sylvite mineral crystals in the biochar (s). K_2SO_4, K_2CO_3, and KCl (sylvite) make up the majority of the K in biochars, whilst $Ca_2P_2O_7$ makes up the majority of P (Dhawane et al., 2018). The peak at 2θ 30.7 was attributed to mineral whitlockite (w) in addition to biochar's calcite (Ca) ($CaCO_3$) content. Whitlockite (beta-tricalcium phosphate), which can also contain magnesium in its structure. The observed results are in tune with observance of P, Ca, and magnesium in EDAX (Mukherjee & Halder, 2016).

The biochars seemed to achieve slight crystalline nature due to the mineral crystallization. The average crystallite size of PWMR, 4PWMR, 6PMWR and 8PMWR calculated by Scherrer equation was observed to be ~2.02 nm, ~42.53nm, ~10.44nm and ~15.34nm respectively.

Scanning Electron Microscopy and Energy Dispersive X-ray analysis:

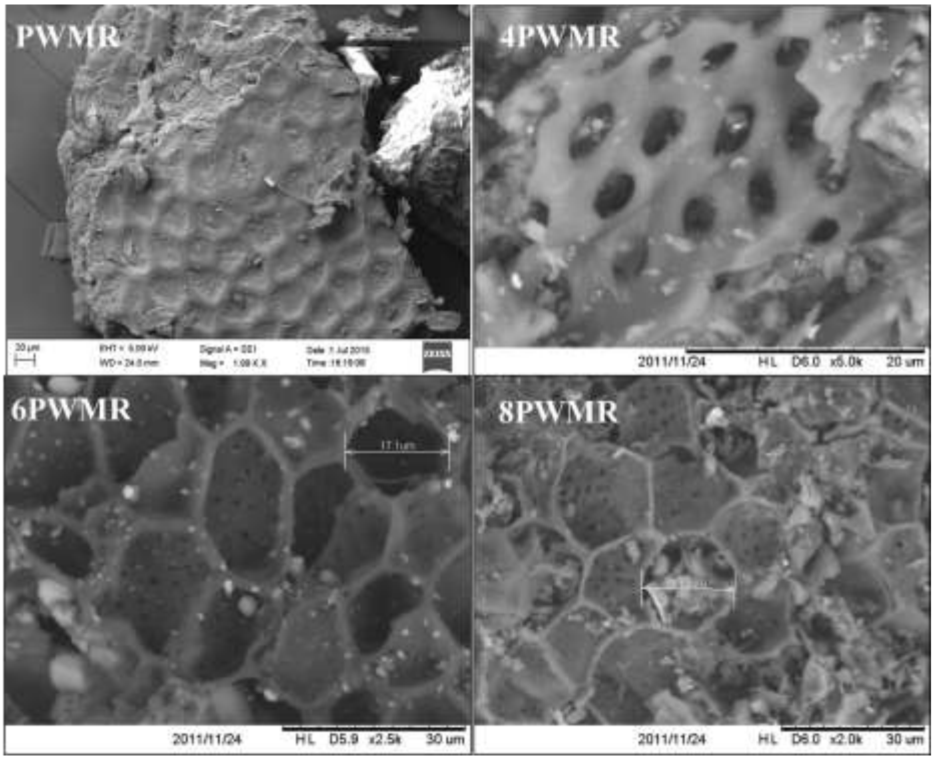

Figure 2.4 SEM images of WMR, 4PWMR, 6PWMR and 8PWMR

SEM images in figure 2.4 shows the morphology of the WMR, 4PWMR, 6PWMR and 8PWMR, which were pyrolyzed at 400ºC, 600ºC and 800ºC respectively. The surface of dried water melon rind (WMR) looked less porous and more compact (figure 2.4a PWMR) as compare to pyrolyzed WMR at different temperature (figure 2.4b. 4c, 4d 4PWMR, 6PWMR and 8PWMR). Biochar pyrolyzed at different temperature exhibited a more rugged surface as compare to PWMR and finally attained a honeycomb like porous structure. It was also observed that pore size increased with increasing temperature, which may increase the uptake of metal, dyes or other pollutants from aqueous solution (Lei et al., 2019). The pyrolysis temperature was observed to affect the microstructure of biochar, consistent with other research reports (Liu et al., 2022)**.**

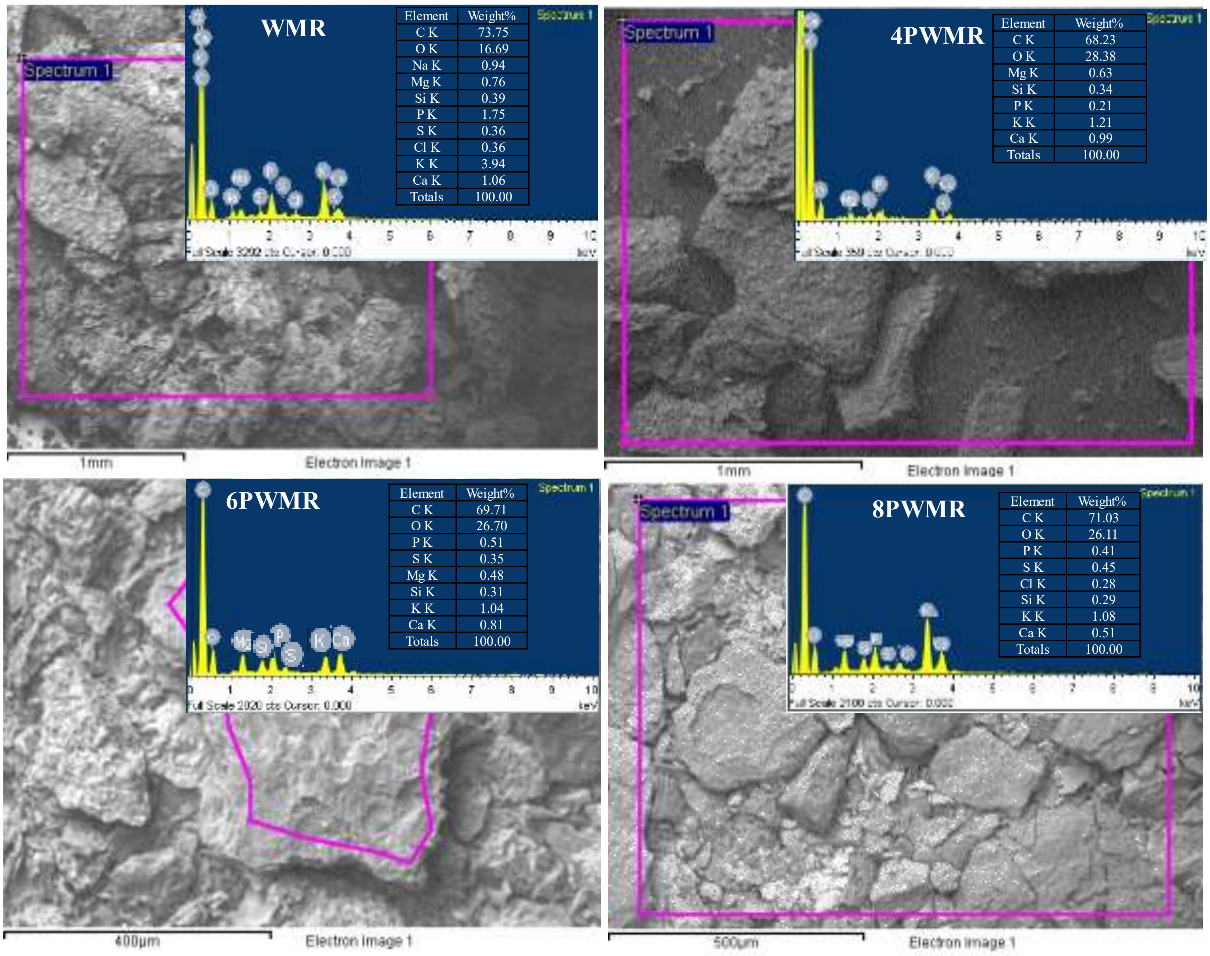

Figure 2. 5 EDAX spectra of WMR, 4PWMR, 6PWMR and 8PWMR

The SEM EDAX, data (figure 2.4 and 2.5) revealed that carbon was the predominant component (68–74%), followed by oxygen (16–28%). Traces of Ca, K, Na, P, S, Mg and Si were also found in all biochars but in very small amounts.

FTIR spectral analysis of biochars

FTIR spectral analyses of WMR and pyrolyzed WMR are shown in figure 2.6. The absorption bands of cellulose and hemicelluloses corresponding to polysaccharides were observed at 1000-1200 cm^{-1} in WMR. The C-H stretching of the aliphatic vibration groups and the O-H stretching of the hydroxyl groups were observed in the range 2980-2820 cm^{-1} and 3200-3400 cm^{-1} respectively. Presence of O-H band confirmed the presence of alcoholic and phenolic functional groups, associated with cellulose as well as hemicellulose and lignin components, present in them respectively. The absorption band at 1030 cm^{-1} depicted the anomeric region of cellulose-like structure and C-O and C-O-C stretching. The C=O stretching of ketones and other carbonyl structures of WMR were observed at 1610-1740 cm^{-1}. The bands observed at

700-850 cm^{-1} were attributed to aryl C-H and/or aryl C-O groups. WMR showed abundant oxygen-containing functional groups on the surface as compared to pyrolyzed WMR at different temperature.

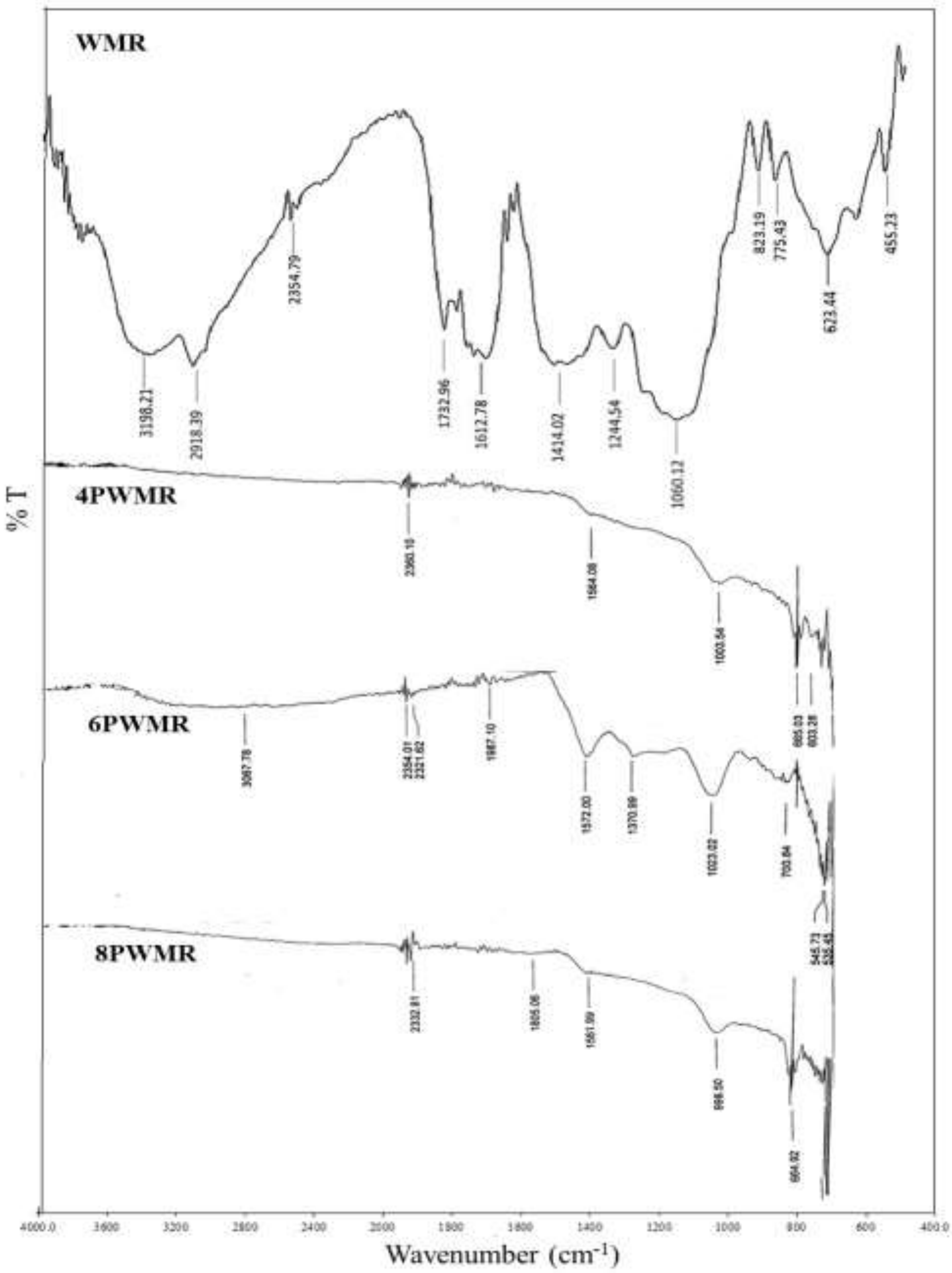

Figure 2.6 IR spectra of WMR, 4PWMR, 6PWMR and 8PWMR

The absorption band observed at 3400-2400 cm^{-1} in WMR disappeared in 4PWMR, 6PWMR and 8PWMR, indicating dehydration and thermal decomposition of cellulosic and ligneous components of WMR (Pasieczna-Patkowska & Madej, 2018). The band between 1600-1614 cm^{-1} can be attributed to vibration of C=O of lactones (Fuente et al., 2003) or carboxyl-carbonate structures (Morterra & Low, 1982). The peaks observed in range 1023-998.50 cm^{-1}

can be attributed to different vibrations including C-O, C-C and C-N single bond stretches as well as C-H bending (Sahoo et al., 2021).

Various out-of-plane C–H deformation bands were observed in the region 900-625 cm^{-1} in 4PWMR, 6PWMR and 8PWMR. These bands can be attributed to solitary aromatic hydrogens in aromatic structures. The absorption bands at 775 cm^{-1} are generally attributed to meta-substituted benzenoid compounds in WMR. The absorption bands at 823 cm^{-1} also are generally attributed to para-substituted benzene ring in WMR. Bands observed at 548-400 cm^{-1} in 4PWMR, 6PWMR and 8PWMR may be attributed to clay and silicate minerals.

2.3.2 Physico-Chemical analysis of Biochars

Investigations were conducted on the physicochemical characteristics of 4PWMR, including its density, pH level, moisture content, Brunauer-Emmett-Teller surface area (BET), ion exchange capacity and iodine sorption values (Table 2.1) (Kushwaha et al., 2013). About 1g of adsorbent was dispersed in 100mL of distilled water and heated the mixture to boiling for 30 minutes while stirring continuously (ASTM 6851). The solution was cooled and pH was determined. A known weight of the sample was heated for approximately 3 h in an air oven maintained at 105°C to measure the moisture content (ASTM D2867). The technique was performed until constant weight was achieved. A previously weighed 100mL graduated cylinder was filled with biochars to the 50mL mark without tapping in order to evaluate the bulk density (ASTM D8176). The biochar cylinder was precisely weighed. The bulk density was estimated by multiplying the weight difference between the biochar-filled and non-biochar-filled cylinders by 50. In order to determine the ion exchange capacity, 100mL of 0.25 M sodium sulphate and 0.5 g of biochar was combined in a stoppered conical flask and shaken in a temperature-controlled bath (ASTM D1193). The mixture was filtered after five hours and the filtrate was then titrated using phenolphthalein against 0.1 N NaOH. The following equation was used to determine the ion exchange capacity of the adsorbent in meq/g:

$$\text{Ion exchange capacity } \left(\frac{\text{meq}}{\text{g}}\right) = \frac{\text{aW}}{\text{V}} \quad \text{…eq. (2)}$$

Where, a= Normality of NaOH

V= Volume of NaOH

W= Weight of the adsorbent in g

Iodine content was determined using iodine adsorption from aqueous solution. It is a relative indication of porosity and is used to compare adsorbent surface areas (Tanaka et al., 2002).

Iodine solution was used to equilibrate around 0.2 g of biochar. Titration with sodium thiosulphate solution was used to calculate the residual iodine concentration.

$\text{Iodine value mg/g} = (\text{Blank} - \text{Burette reading of sample}) \times \text{Conversion factor}$…...eq.(3)

$\text{Conversion factor} = \frac{\text{Mol.Wt.of Iodine } (127)\times 40}{\text{Wt.of Carbon}\times\text{Blank Reading}}$ …………………………………………eq.(4)

where the blank reading is the burette reading for the iodine concentration without adding an adsorbent and the burette reading is for the iodine that is still in the solution after adding charcoal but has not yet been absorbed.

By using a BET surface area analyser at 77.3 K, the porosity of the 4PWMR was measured. The BET equation was used to compute the specific surface area from the isotherm:

$\frac{1}{v\left[\left(\frac{P_0}{P}\right)\right]-1} = \frac{C-1}{v_m C}\left(\frac{P}{P_0}\right) + \frac{1}{v_m C}$ ………………………………………………………………eq.(5)

P and P_0 are the equilibrium and saturation pressures of the adsorbate at the adsorption temperature, v is the amount of gas adsorbed (in volume units), v_m is the volume of gas adsorbed in a monolayer and c is the BET constant, which is written as:

$c = \exp\left(\frac{E_1 - E_L}{RT}\right)$……………………………………………………………………………eq.(6)

Table 2. 1 Physico-Chemical properties of the Adsorbent

Parameters	4PWMR	6PWMR	8PWMR
pH	9.2	9.0	8.9
Moisture content	10.39 %	0.432 %	0.319 %
Bulk density	0.4921 g/mL	0.5321 g/mL	0.7865 g/mL
Ion exchange capacity	0.033 meq/g	0.054 meq/g	0.093 meq/g
Iodine value	389.93 m^2/g	421.83 mg/g	479.25 mg/g
BET surface area	0.5365 m^2/g	6.46 m^2/g	177 m^2/g

2.4 Adsorptive removal of fluoride using 4PWMR

2.4.1 Experimental methods

2.4.1.1 Materials and methods

Sodium fluoride (NaF) obtained from Spectrochem were used in this study without further purification.

Fluoride stock solutions were made by dissolving 2.2105 g sodium fluoride (Spectrochem) in 1000 mL of conductivity water and then diluting to the desired concentration.

Preliminary experiments revealed that there was no significant difference in uptake of PWMR at different temperatures while use of WMR resulted in some leaching of color into the solution. To make the adsorptive process cost effective it was decided to use 4PWMR for further defluoridation studies.

The fluoride uptake experiments were carried out in batch mode, with a known weight of 4PWMR dispersed in a 100 mL polypropylene flask containing fluoride at concentrations ranging from 1 to 100mg/L. The flasks were orbitally shaken at a constant rate of 150 rpm for 3h at room temperature (35$\pm$2^{o}C). After a desired time interval, the adsorbent was filtered and dried for further analysis. The fluoride remaining un-adsorbed in the solution was measured by a fluoride ion selective electrode (Thermo scientific ORION STAR A214)., provided by Metroohm from a calibration graph plotted by analysing known concentrations of fluoride standard solutions TISAB IV buffer (15 mL provided by Metrohm was used to maintain the pH at 5-7. The following formula was used to determine how much fluoride was absorbed:

$q_e=C_i-C_e/m*100$ ………………………...……………………………………eq. (1)

where q_e is the fluoride uptake (mg/g), C_i is initial fluoride concentration (mg/L), C_e is equilibrium fluoride concentration (mg/L) and m is mass of the adsorbent (mg).

All experiments except pH variation studies were conducted at pH 1.

To comprehend the adsorption process, the experimental data were fitted to various isotherm and kinetic models (table 2.2). Further investigations were done into the regenerability, reusability and applicability of 4PWMR for defluoridation of industrial effluents and ground water samples.

Table 2. 2 Isotherm and kinetic models

Isotherm	Functional form	Linear form	plot

Freundlich	$q_e = K_f C_e^{1/n}$	$log q_e = \log k_F + \frac{1}{n} log C_e$	LogC_e vs Log q_e
Langmuir	$\frac{q_e}{q_m} = \frac{K_L C_e}{1 + K_L C_e}$	$\frac{C_e}{q_e} = \frac{1}{q_m} C_e + \frac{1}{k_L q_m}$	$C_e\ vs\ \frac{C_e}{q_e}$
Pseudo 1st order	$\frac{dq}{dt} = K_i'(q_e - q_t)$	$\log(q_e - q) = \log(q_e) - \frac{K_1 t}{2.303}$	$t\ vs$ Log $(q_e - q_t)$
Pseudo 2nd order	$q_t = \frac{q_e^2 K_2' t}{1 + q_e K t}$	$\frac{t}{q_t} = \frac{1}{K_2 q_e^2} + \frac{t}{q_e}$	$t\ vs\ \frac{t}{q_t}$
Intraparticle Diffusion	$\boldsymbol{q_t = K_i t^{0.5}}$	$\boldsymbol{q_t = K_{id} t^{0.5} + C_i}$	$\mathbf{t^{0.5}}\boldsymbol{vs\ q_t}$

2.4.2. Fluoride uptake studies

2.4.2.1 Effect of pH

At an initial fluoride concentration of 50 mg/L, the influence of pH on the adsorption of fluoride onto 0.1 g of 4PWMR was examined (figure 2.7a) in the pH range of 1.0-11.0. Maximum adsorption was seen at pH 1, with a rapid decline in adsorption effectiveness above pH 2.

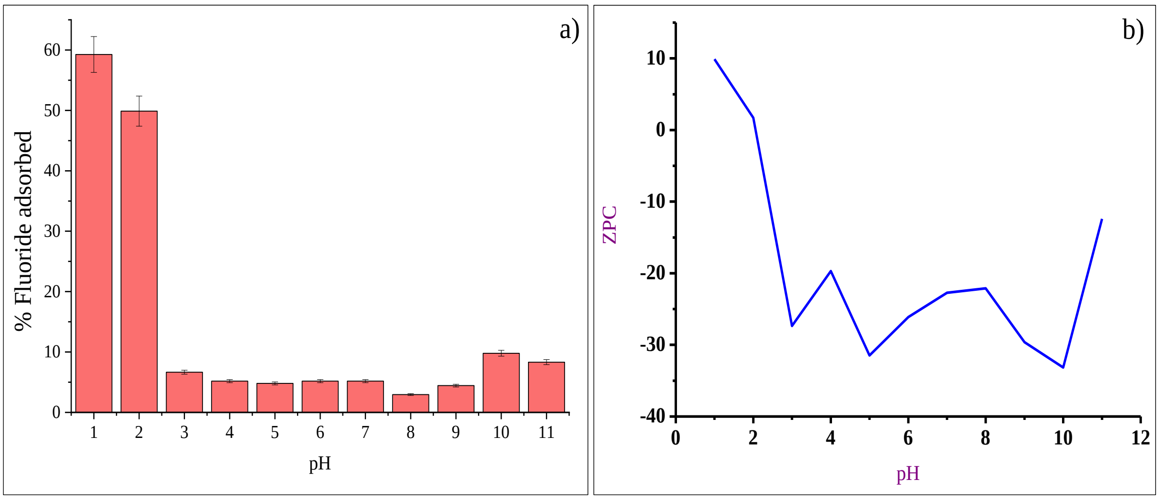

Figure 2.7 a) Effect of pH on removal of fluoride (contact time: 3 h, dose: 0.1g, initial fluoride concentration: 50mg/L) (b) ZPC of 4PWMR

At low pH higher hydronium ion concentrations will protonate the basic functional groups of 4PWMR, enabling them to bind fluoride ions. Dinesh et al. made comparable observations in his investigations of fluoride removal by pine bark and pine wood (Zhou et al., 2019). These protonated functionalities attract the hydrated fluoride ions. More hydrated H_3O^+ F^- ion pairs may migrate into the biochar's pore walls and exchange with protonated functionalities present there (Patel et al., 2009).

By evaluating the zeta potential of 4PWMR as a function of pH, the change in surface charge of the adsorbent was examined to further understand this observation. The surface charge of the adsorbent was found to be negative above pH 2.1 which was the zero-point charge of 4PWMR (figure 2.7b).

Less protonated sites would be present as pH was raised, making fluoride removal less effective. The electrostatic rejection of fluoride ions by the negative surface charge on 4PWMR may be the cause of the decrease in fluoride removal in alkaline circumstances (Zhou et al., 2019).

2.4.2.2 Effect of dose

To examine the impact of 4PWMR dose on the efficacy of defluoridation of 25mL of 50 mg/L fluoride containing solution, batch sorption experiments with various doses of 4PWMR (0.025-0.2 g) have been conducted. Due to the increased availability of active sites, it was found that fluoride uptake increased with an increase in 4PWMR dosage (figure 2.8a).

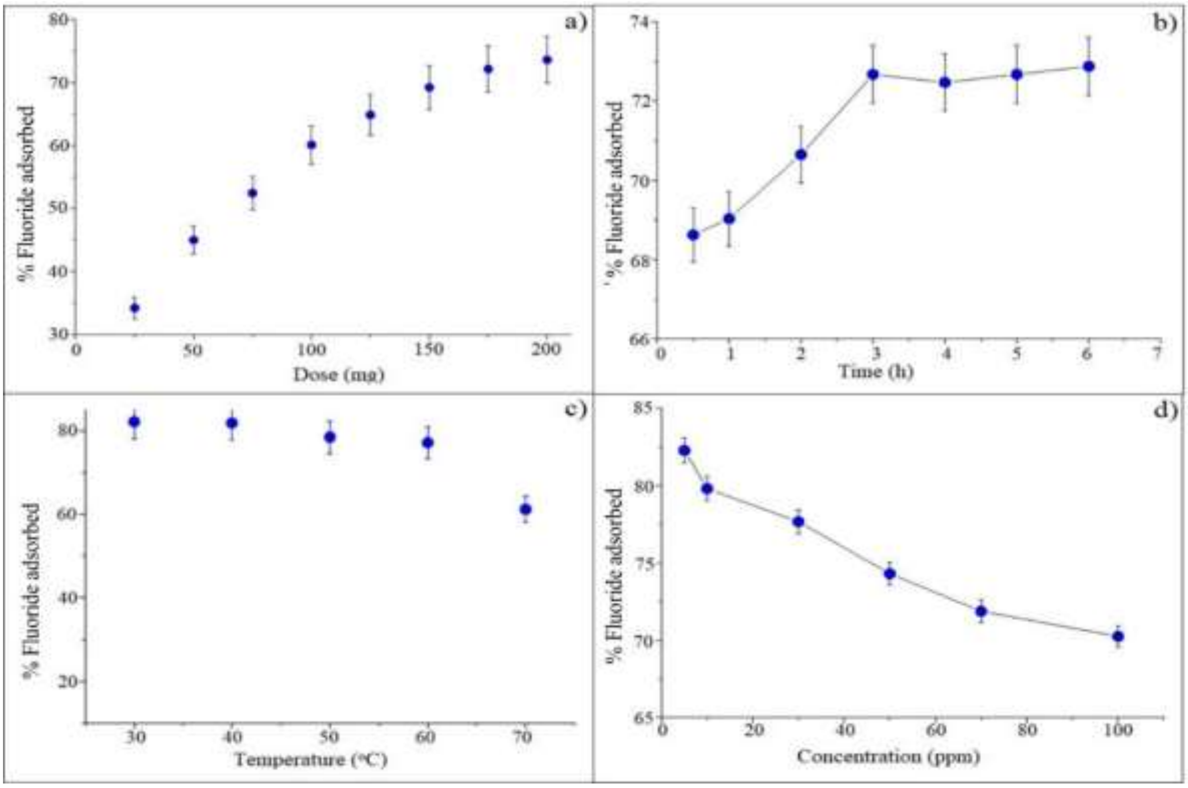

Figure 2.8 Effect of a) adsorbent dose b) contact time c) temperature and d) initial concentration of fluoride on % uptake of fluoride (contact time: 3h for a, c and d; initial fluoride concentration: 50mg/L for a b and c; pH 1)

2.4.2.3 Effect of contact time

The effect of contact time was examined by equilibrating 25 mL of a 50mg/L fluoride solution at pH 1 with 0.2g of 4PWMR for various time periods (figure 2.8b). After 3h of equilibration, the maximum uptake was seen and continued to be consistent. In the first half hour, a sizable portion of fluoride (66 %) was eliminated and after that the removal rate gradually rose until equilibrium was attained. The fact that all adsorbent sites were initially unoccupied and the solute concentration gradient was large may have contributed to the shift in the rate of removal. Later, as the number of adsorption sites and fluoride concentration both dropped, the rate of fluoride uptake by the adsorbent dramatically decreased (Sujana & Anand, 2011).

2.4.2.4 Effect of temperature

The impact of temperature on fluoride uptake is seen in figure 2.8c. Since adsorption steadily decreased as temperature rose, this indicated that the adsorption process was exothermic. The reduced adsorption may be brought on by the molecules' greater propensity to escape off the adsorbent surface and into the solution phase, which causes the boundary layer's thickness to decrease (Z. Jin et al., 2015).

2.4.2.5 Effect of initial concentration of fluoride

Figure 2.8d shows the results of an investigation into the impact of the initial fluoride concentration (5 to 100 mg/L) on the adsorption process. Due to the lack of available active sites, it was shown that fluoride uptake reduced as fluoride concentration increased.

To further model the experimental data, Langmuir, Freundlich, Temkin and Halsey isotherms were also applied. Table 2.3 and figure 2.9 display the results of fitting experimental data to these four models and the sorption parameters.

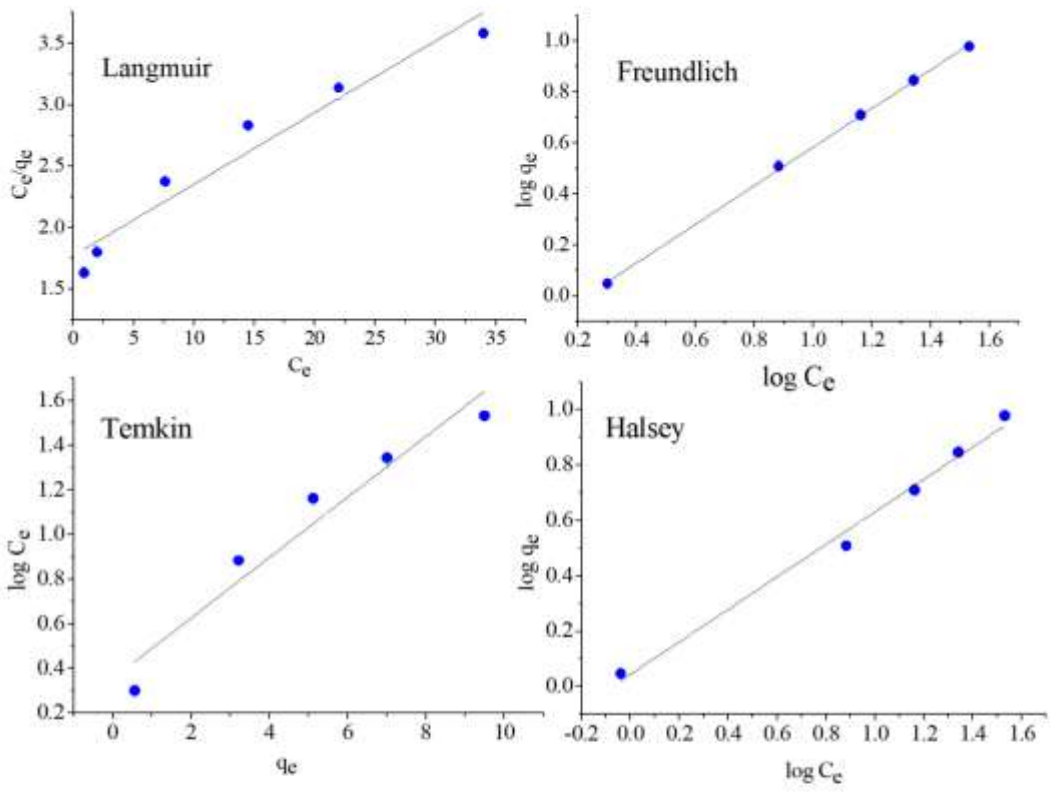

Figure 2.9 Isotherms of fluoride uptake by 4PWMR

In comparison to the Langmuir model, the Freundlich model provided a better fit (r^2= 0.9989 vs. 0.9479), showing that the adsorption process was occurring on a heterogeneous surface that changed with surface coverage (Bell, 2011). Additionally, the computed value of n from the slope of the Freundlich isotherm plot was 1.28, indicating favourable adsorption (Bell, 2011).

The uniform distribution of binding energies in the Temkin isotherm (Başar, 2006) is one of its characteristics. The following values were estimated using the Temkin plot depicted in figure 2.9: b_T = 0.1016 and A_T = 0.598 L/g indicating a physical adsorption mechanism.

The Halsey adsorption isotherm is appropriate for multilayer adsorption (Rehrah et al., 2014) and the experimental data's fitting to this model revealed the adsorbent's hetero porous nature.

Table 2.3 Isotherm parameters of Langmuir. Freundlich, Temkin and Halsey for the adsorption of fluoride by 4PWMR

	Isotherm Parameters		
Langmuir	Q_m	K_L (L.mmol^{-1})	r^2
	20.44	0.0328	0.9479
Freundlich	N	k_F(L.g^{-1})	r^2
	1.2799	0.6282	0.9989
Temkin	A_T (Lg^{-1})	b_T	r^2
	0.5980	0.1016	0.97
Halsey	k_H (L.g^{-1})	n_H	r^2
	0.8405	-1.7024	0.9900

The adsorption capacity of 4PWMR was found to be greater than that of previously reported biochars, groundnut shell, manganese oxide coated alum and agricultural waste. While aluminium hydroxide-based adsorbents, carbon and sweet lime performed better. However, comparing the efficiency of adsorbents is difficult because sorption capacities have been reported at various pH, temperatures, adsorbent doses, adsorbate concentration ranges, adsorbent particle size and surface areas.

It is also difficult to compare the material's economic feasibility to that of previously reported biochars due to differences in preparation conditions, properties, applications and adsorption capacities. However, we followed the common methodology for biochar preparation by optimising the slow pyrolysis technique at low temperatures.

Table 2.4 summarises the comparison of adsorption capacity of various adsorbents reported in the literature for fluoride removal.

Table 2.4 Comparison with other reported adsorbents

Adsorbent	pH	q_{max}(mg/g)	Ref.
Waste carbon slurry	7.58	4.15	(Lee et al., 2013)
Banana peel	6	17.4	(Singh, 2015)
Groundnut shell	7	1.15	(Jawad et al., 2019)
Sweet lemon peel	2-12	59.59	(Khan et al., 2015)
Agricultural waste	6	6	(Gerçel et al., 2007)
Mushroom compost biochar coated with aluminum hydroxide	6-8	36.5	(Budyanto et al., 2015)
Distiller's grains biochars coated by aluminum hydroxide	5-9	18.05	(Budyanto et al., 2015)
Activated Biochar of Colocasiaesculenta Stem	4.25	7.3	(Kishore, 2011)
Steam-Activated Biochar Derived from Cocosnucifera Shell	6.5	0.95	(Sadhu et al., 2022)
Corn stover biochar	2	5.0	(Kishore, 2011)
Magnetic corn stover biochar	2	3.41	(Kishore, 2011)
Pine wood biochar	2	7.66	(Mohan et al., 2012a) (Mohan et al., 2012b)
Pine Bark biochar	2	9.77	(Mohan et al., 2012a)
Hydrous manganese oxide-coated alum	4-6	7.09	(Teng et al., 2009)
Zirconium based metal organic frame works	-	19.42	(Tan et al., 2020)
Laponite clay	7	10.8	(Braik et al., 2022)
4PWMR	1	20.44	This study

2.4.2.6 Adsorption kinetics and thermodynamics

Pseudo-first-order, Pseudo-second-order, Elovich, and Intraparticle diffusion models were used to analyse the kinetic data (figures 2.10). Table 2.5 contains the derived rate constants and r^2 values.

It was noted that the experimental qe values of the pseudo-second order equation were closer to the computed qe values than the pseudo-first order equation. The pseudo-second order model's regression coefficient (r^2) value at 303 K was 0.9989, indicating that it provided the greatest fit kinetically and that some chemical interactions as well as physical ones contributed to the binding of 4PWMR and fluoride (Teng et al., 2009).

Second order kinetics was described by the Elovich equation under the assumption that the actual solid surfaces are energetically heterogeneous (Ho & McKay, 1998). Higher value of A (46100.35) than B (4.0633) suggested higher adsorption rate than desorption, indicating a viable adsorption process [73].

The sorbate concentration-square-root-of-time plot of the intra-particle diffusion model gave an r^2 values of 0.9315, indicating that intraparticle diffusion was also regulating the adsorption process.

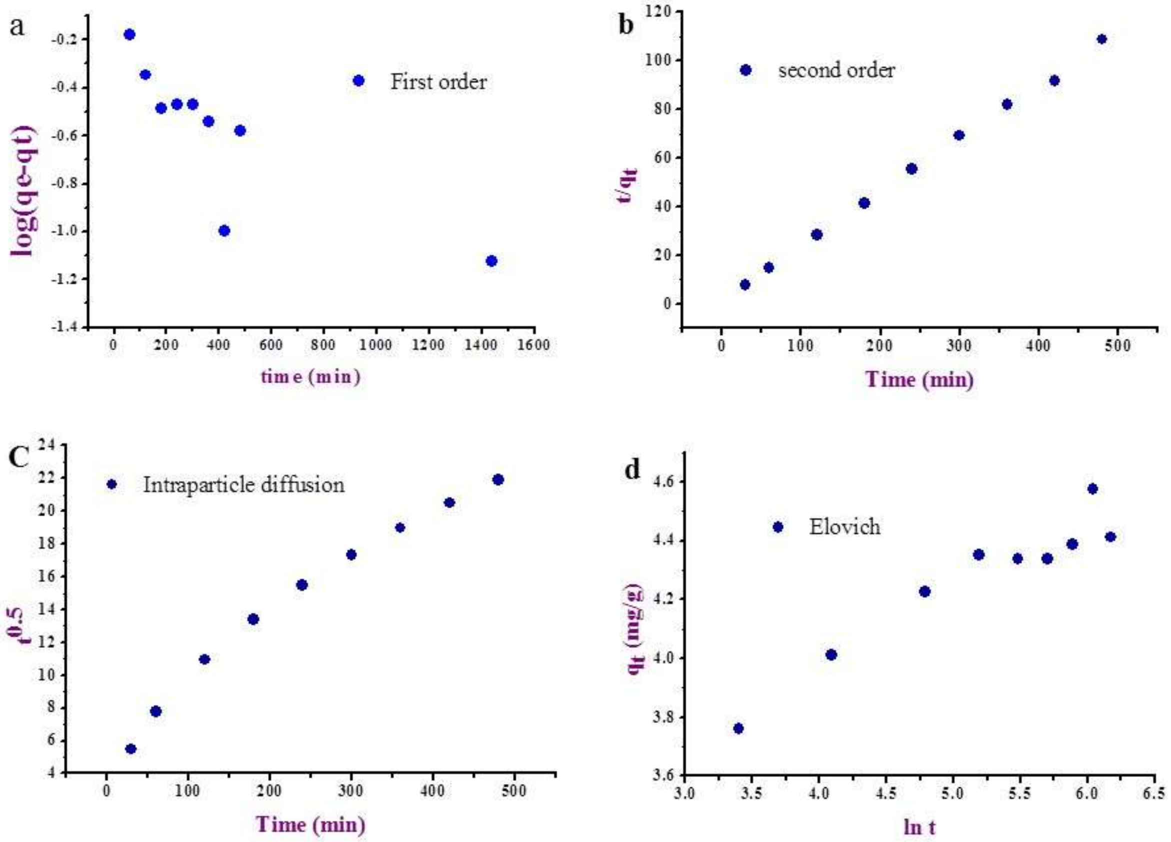

Figure 2.10 Kinetic models for fluoride adsorption onto 4PWMR

Table 2.5 Kinetic parameters of Pseudo first order, Pseudo Second Order, Intraparticle diffusion and Elovich models for the adsorption of fluoride onto 4PWMR

q_e(exp): 4.675mg/g	q_e	K	r^2	A	B
Pseudo First order	0.7719	0.0032	0.7977		
Pseudo Second order	4.5269	1.7916	0.9989		
Intraparticle diffusion	10.5979	0.0216	0.9315		
Elovich	5.0676		0.9164	46100.35	4.0634

The thermodynamic parameters for fluoride adsorption, including change in free energy (G°), enthalpy (H°), and entropy (S°), are shown in table 2.6.

Table 2. 6 Thermodynamic Parameters of fluoride adsorption onto 4PWMR

Thermodynamic parameter	Value
ΔG	-22.28 kJ/mole
ΔS	0.039 KJ mol^{-1} K^{-1}
ΔH	-10.46 KJ

The exothermic nature of adsorption accounts for the negative value of enthalpy, while the negative value of free energy revealed the process's viability and spontaneity. The G° results from this investigation were greater than 20 kJ/mol, showing that charge sharing or charge transfer was the main mechanism in the sorption process (Ho & McKay, 1998).

2.4.2.7 Effect of competing anions

Natural water often contains a number of anions. Figure 2.11a illustrates the evaluation of the influence of co-existing anions (such as Cl^-, NO_3^-, SO_4^{2-}, HCO_3^-, and CO_3^{2-}) on fluoride adsorption by 4PWMR. Using 8 g/L of 4PWMR in 50 mg/L of fluoride solution containing 50 mg/L and 100 mg/L of various anions, fluoride absorption over 4PWMR was examined. The stated anions barely had any impact on the adsorption of fluoride. In the presence of anions that were twice as concentrated as fluoride, the adsorption capacity of 4PWMR for 50 mg/L fluoride dropped by about 5-7 percent.

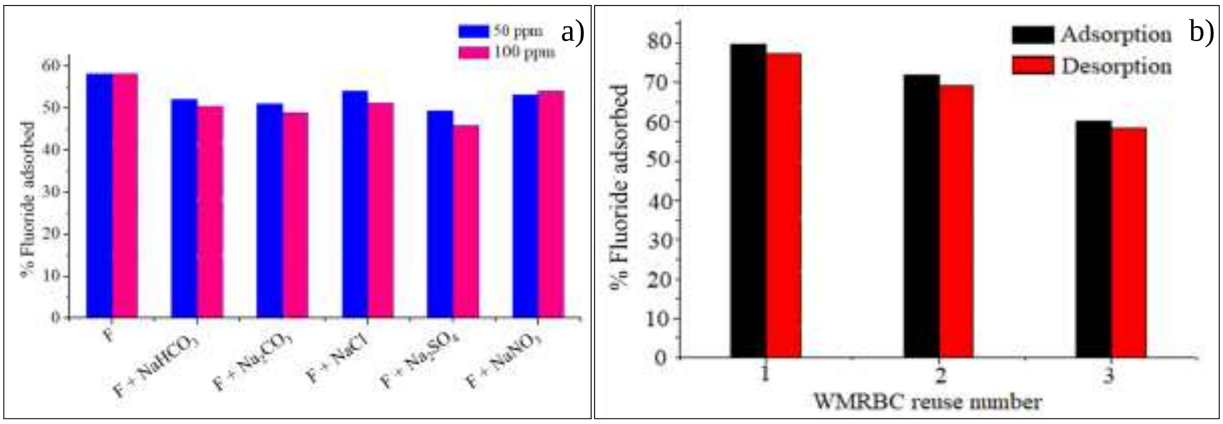

Figure 2.11 a) Effect of competing anion concentration on % uptake of fluoride, b) Uptake of fluoride after consecutive 1st 2nd and 3rd cycle using 0.1N NaOH as regenerant (Initial dose: 0.02 g, pH 1, initial fluoride concentration: 50 mg/L)

2.4.2.8 Reuse of adsorbent

To investigate the desorption and regeneration of 4PWMR, three consecutive adsorption-desorption cycles were carried out. Using 0.1M NaOH solution, desorption was reported to be 77.11 percent. For the first, second and third cycles of batch operations, the percent uptake of fluoride was observed to be 79.54 percent, 71.99 percent and 60.17 percent, respectively (figure 2.11b). The findings demonstrated the applicability and viability of adsorbent for industrial applications.

2.4.3 Characterization of 4PWMR after adsorption of fluoride

Scanning electron microscopy and Energy dispersive X-ray analysis:

The EDAX analysis of 4PWMRF are shown in the insets of figure 2.12. Fluoride peak's appearance in EDAX spectrum suggested that fluoride was successfully adsorbed onto 4 PWMR. The significant rise in S and O content in 4PWMRF could be attributed to the uptake of sulphate ions in water along with fluoride after 3 hours of agitation at pH 1.

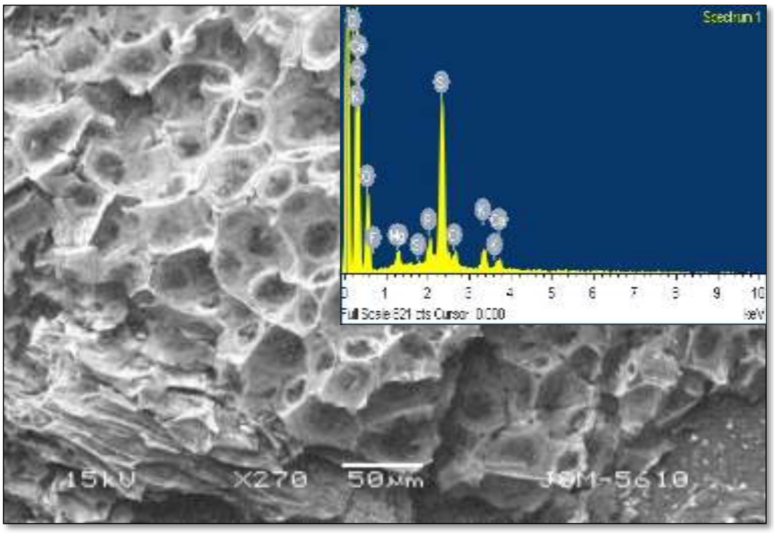

Figure 2. 12 SEM images of after adsorption with insets depicting EDS spectra of 4PWMR after adsorption

The results of the XRD examination, along with the FITR spectra and EDAX analysis, showed that the inorganic component of the biochar samples was primarily composed of carbonate and phosphate-rich species.

FTIR spectral analysis

Figure 2.13 shows the equivalent spectra from the IR spectral analysis of the 4PWMRF. Due to the partial chemical transformations that take place at low pyrolysis temperatures, biochars have been seen to act like feedstocks by preserving a specific level of hydration and a carbohydrate structure (Schwanninger et al., 2004).

Following fluoride adsorption, the bands resulting from C-H stretching vibrations of the methyl and methylene groups, which were observed at 2984 cm^{-1} and 2894 cm^{-1}, respectively, in pure 4PWMR, have been shifted to 2981 and 2896 cm^{-1}, along with the appearance of a new peak at 997 cm^{-1} indicating C-F stretching (Kushwaha et al., 2013). However, the biochar might likely retain the absorption intensities around 1610-1740 cm^{-1}, which correspond to C=O stretching of ketones and other carbonyl compounds (Schwanninger et al., 2004) of pristine WMR.

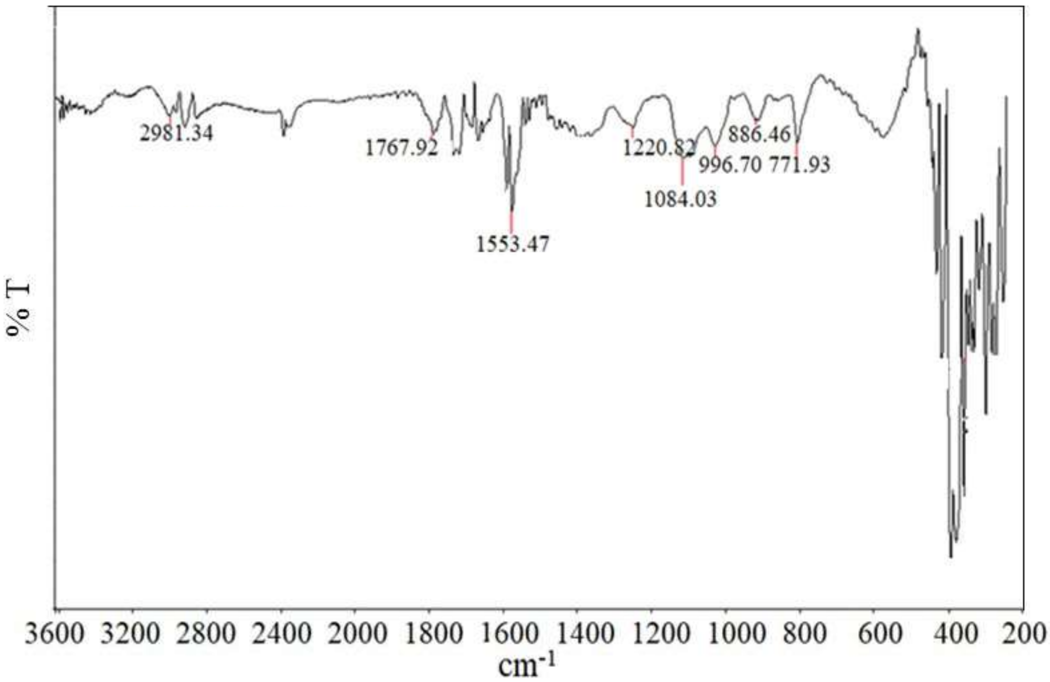

Figure 2. 13 IR spectra of 4PWMRF

2.4.4. Discussion

The fluoride adsorption capability of 4PWMR could not match its surface area (0.5365 m^2/g). This suggested that the adsorption process must involve a number of different mechanisms. Below are some potential mechanisms that have been suggested:

a) The Temkin isotherm model's low heat of adsorption result (0.1016 J/mol) demonstrated the physical nature of the adsorption process. Van der Waals forces are one of the main ways that physical adsorption can happen (Başar, 2006).

b) The biochar was found to contain metals such Mg, Ca, Si and K, which can form bonds with fluoride and lead to the production of insoluble fluoride on the adsorbent, according to XRD and EDS data.

c) Both the inside and outside of the biochar have been found to contain a wide range of oxygen-containing functional groups, including those that can be protonated and used to bind fluoride electrostatically, such as hydroxy, anhydride, carboxylic acid, ketone, quinone, ether, lactone and pyrone (N. et al., 2012).

d) Kumar et al. (H. Kumar et al., 2019) have described the possibility of an ion exchange process using anions coupled with quaternary ammonium groups, if any. However, EDAX experiments conducted for this work have revealed the presence of chloride on both the 4PWMR before and after fluoride adsorption, indicating that ion exchange did not take place. Dehydrated hemicellulose and cellulose residues have been found in TGA and IR experiments and these can cause an electrophilic carbon to form on the surface of biochar.

2.4.5 Conclusion

In this study, watermelon rind biochar (4PWMR) was characterised and used to effectively remove fluoride ions from water. The ideal pH and contact time for adsorption, according to batch tests are 1 and 3 hours, respectively. The Freundlich isotherm model and pseudo second order kinetics were better fits for the adsorption data. The spontaneous and exothermic nature of the adsorption process was shown by the negative values of free energy and enthalpy. 4PWMR has a maximum fluoride adsorption capability of 20.44 mg/g at pH 1. The pH of the treated water would need to be adjusted, which would necessitate the addition of Na_2CO_3, $MgCO_3$ and $CaCO_3$. Modification of 4PWMR to make it more amenable for removal of fluoride at neutral pH would be a part of our future studies. The effectiveness of the adsorbent in defluoridation of both industrial wastewater and ground water was demonstrated. Common co-existing anions like Cl^-, NO_3^-, SO_4^{2-}, HCO_3^-, and CO_3^{2-} had little impact on capacity of 4PWMR to adsorb fluoride. Furthermore, after being recycled three times, 4PWMR still retained around 60% of its original adsorption capability. Metals like Mg, Ca, Si, and K were found in biochar during its XRD and EDS characterization, which could help in the development of insoluble fluoride on the adsorbent. Numerous oxygen-containing functional groups that are amenable to protonation and electrostatic binding with fluoride were found, according to FTIR analyses. Thus, the elimination of fluoride was mostly ascribed to the interaction of metal fluoride precipitation and electrostatic attraction.

2.5 Adsorptive removal of Methylene blue using Watermelon rind derived biochar

Preliminary experiments conducted on the removal of methylene blue indicated 8PWMR to be a better adsorbent for methylene blue removal and hence further investigations were done using 8PWMR.

2.5.1 Experimental methods

2.5.1.1 Materials

Methylene blue ($C_{16}H_{18}N_3SCl.3H_2O$) obtained from Spectrochem was used in this study without further purification.

2.5.2 Methylene blue uptake studies:

Stock solution of MB was prepared by dissolving 1000 mg methylene blue (make Spectrochem) in 1000 mL of conductivity water to make 1000 ppm solution. The MB uptake studies were conducted in batch mode by using 4 g/L ratio of 8PWMR for 100 mg/L to 1000 mg/L of dye solution in 100 ml conical flask at room temperature. The flasks were shaken at a constant rate of 150 rpm for 2 h in rotary mechanical shaker.

The residual concentration of dye was measured using UV visible spectrophotometer (make JASCO). The calibration spectrum was recorded by analysing known concentration of dye solution from which the unknown concentration of dye was determined. The amount of dye uptake was calculated using the formula: q_e=C_i-C_e/m*100 where q_e is the dye uptake (mg/g), C is initial dye concentration(mg/L), C_e is equilibrium dye concentration (mg/L), V is volume of solution (L) and m is mass of the material (mg).

The effect of pH on the adsorption capacity of 8PWMR was evaluated in the pH range of 1-11. Initial pH of the dye solution was adjusted using 0.1 M NaOH and 0.1 M HCl. Other experiments were conducted at neutral pH. The effect of dose of adsorbent was studied by varying dose in range of 0.08 to 0.48 g/L.

The experimental data were fitted to several isotherm and kinetic models (Table 1) to understand the adsorption process.

2.5.2.1 Effect of pH

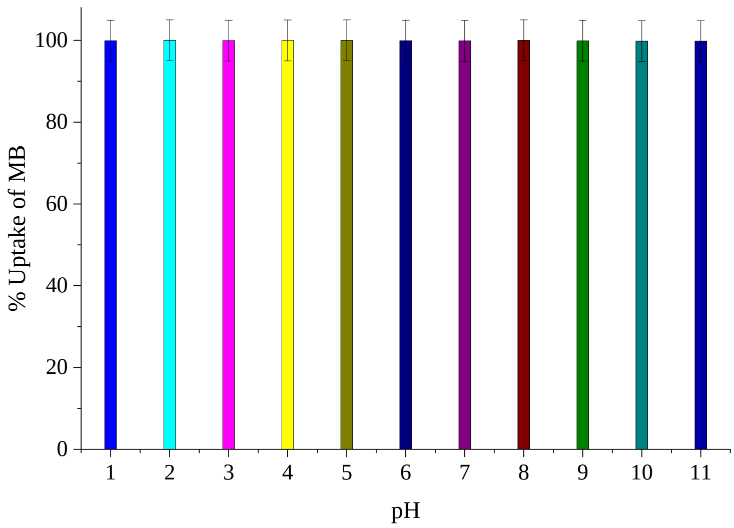

Figure 2.14 Effect of pH on % uptake of MB (contact time: 2 h, dose: 0.1g, initial dye concentration: 100ppm)

The effect of pH on adsorption of dye on to 8PWMR is considered to be important due to competitive adsorption for active sites by H^+ ions. On the basis of FTIR spectral analysis, different functional groups like hydroxy, carbonyl, carboxyl, phenolic etc. were observed which may be involved in potential binding process. This study was investigated in the pH range 1.0–11.0 (figure 2.14) at an initial dye concentration of 100 mg/L using total aqueous solution of 25 mL and agitating for 2 h. It was observed that the adsorption process was independent of pH of the MB solution. This may reveal that electrostatic attraction was not the predominant mechanism operating during the adsorption process. Further experiments were carried out at pH 7.

2.5.2.2 Effect of dose

The effect of adsorption dose was studied by varying the 8PWMR dose between 0.02 g to 0.12 g by taking 25 mL of 200 mg/L solution of MB (figure 2.15). The % uptake of MB increased as the adsorbent dose was increased from 0.02 to 0.1 g. However, with further increase in dose uptake remained almost constant because of the aggregation of adsorption sites which results in a decrease in total adsorbent surface area available to the adsorbate and also increased diffusion path length.

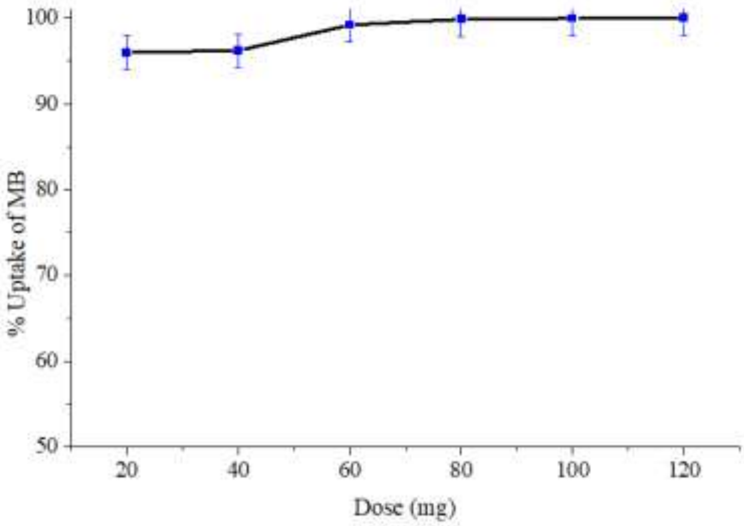

Figure 2.15 Effect of dose on % uptake of MB

2.5.2.3 Effect of contact time

The adsorption data for the removal of MB versus contact time for 200 mg/L MB dye is presented in figure 2.16. The experiments were performed by taking 25 mL of dye solution equilibrating with 0.05 g of 8PWMR for different time intervals. The dye adsorption increased with increase in contact time and remained almost constant after an equilibrium time was reached. Maximum uptake was observed within 30 mins. Significant fraction of methylene blue (>90%) was removed in the first 5 mins and then increased until equilibrium was reached. This observation may be due to the fact that initially solute concentration gradient was high and also the adsorbent sites (pores of right size) are available.

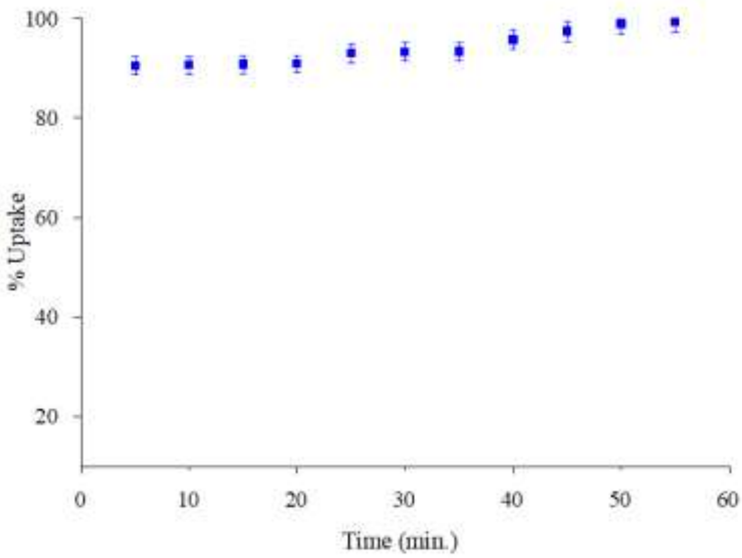

Figure 2.16 Effect of contact time on % uptake of methylene blue (dose: 0.05 g, initial concentration: 200 ppm)

2.5.2.4 Effect of temperature

The effect of temperature on the adsorption of methylene blue using 0.05 g 8PWMR in 25 mL of solution containing 200 mg/L MB, at 60 min of contact time was investigated (figure 2.17). It was observed that there was no significant change in uptake when temperature was raised from 30°C to 60°C. The maximum removal dye percentage at 30°C, 40°C, 50°C, 60°C was found to be 99.97, 99.98, 99.95 and 98.98% respectively.

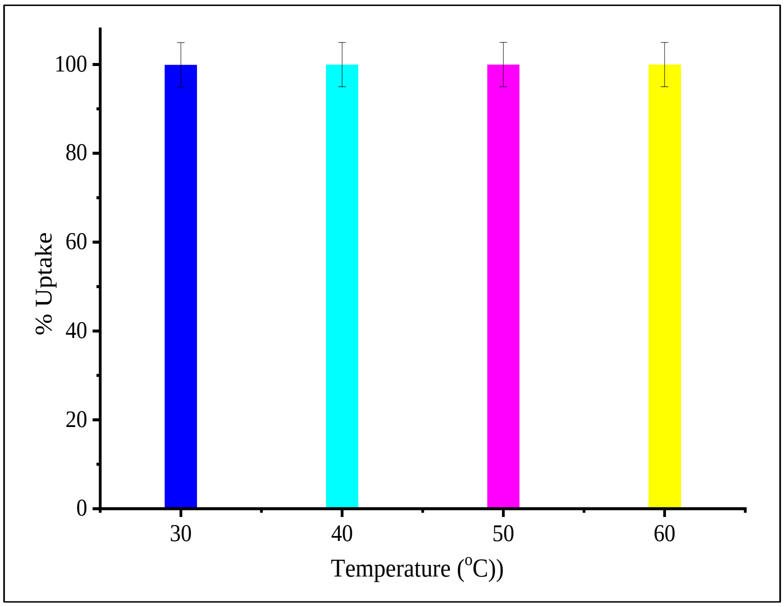

Figure 2.17 Effect of temperature on % uptake of methylene blue (dose: 0.05 g, initial methylene blue concentration: 200ppm, contact time: 1 h

2.5.2.5 Effect of initial concentration of dye

Effect of initial MB concentration (50 to 1000 mg/L) on the adsorption process was investigated and is shown in figure 2.18. It was observed that there is only slight decrease in the uptake of dye with increase in concentration. Since the initial MB concentration increased from 50 to 1000 mg L^{-1} the equilibrium percentage dye removal decreased from 99.87 to 98.20%. This may be attributed to the fact that at low concentrations the ratio of surface-active sites to the total dye molecules in the solution is high and hence all dye molecules may interact with the activated carbon. At higher concentrations the MB may form dimers on the surface and get adsorbed.

Further the adsorption data were fitted with adsorption isotherm models which shows the distribution of adsorption molecules between the solid phase and liquid phase when the adsorption process reached its equilibrium state.

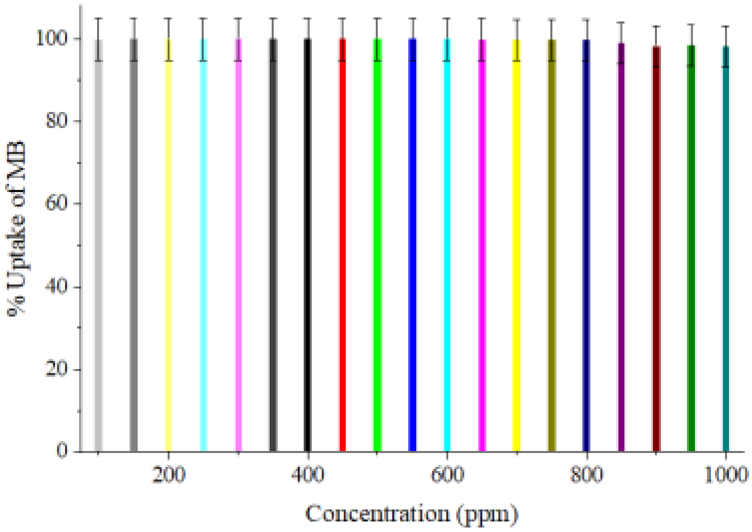

Figure 2.18 Effect of initial dye concentration on % uptake of methylene blue (dose: 0.1 g, contact time: 2 h)

Table 2. 7 Isotherm parameters

	Isotherm Parameters		
Langmuir	Q_m	K_L (L.mmol^{-1})	r^2
	238.09	2.47	0.99
Freundlich	N	k_F(L.g^{-1})	r^2
	1.19	172.70	0.97
Temkin	A_T (Lg^{-1})	b_T	r^2
	-2.4505	0.0152	0.95
Halsey	k_H (L.g^{-1})	n_H	r^2
	168.66	-0.118	0.93

The Langmuir model endorsed that the adsorption occurred at specific homogeneous sites on the adsorbent (Armbruster & Austin, 1938). Whereas the Freundlich model assumes the heterogeneity of the surface and states that the adsorption occurs at sites with different energy levels of adsorption (Armbruster & Austin, 1938). The results of the experimental data fitted better to Langmuir isotherm model as compared to Freundlich, Temkin and Halsey models and its parameters are shown in Table 2.9 and figure 2.19. Further, the value of *n* calculated from the slope of the plot of Freundlich isotherm was 1.19 for MB suggesting favourable adsorption (Bell, 2011). The Temkin isotherm parameters indicated a negative binding constant and hence is not a good fit as also affirmed by temperature studies which indicated the adsorption process to be independent of temperature.

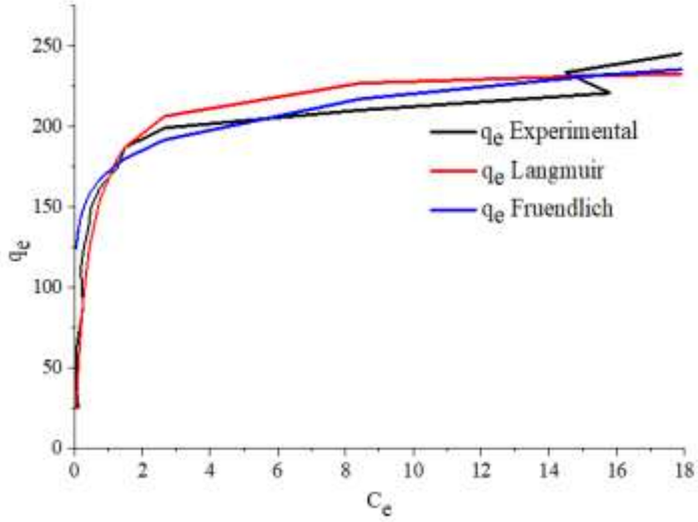

Figure 2.19 Comparision of q_e value with the experimental value of Langmuir and Fruendlich isotherms

Table 2. 8 Comparison of Adsorption Capacities of various adsorbents for methylene blue removal

Adsorbent	pH	q_{max}mg/g	Ref.
Activated carbon from Ficuscaricabast	8	47.62	(Pathania et al., 2017)
steam activated bituminous coal	11	580	(El Qada et al., 2006)
Activated carbon from *Posidonia oceanica* (L.) dead leaves	Adsorption Unaffected by pH of solution	285.7	(Dural et al., 2011)
Activated Carbon Prepared from Pea Shells	6.85	246.91	(Geçgel et al., 2013)
Activated carbon produced from tea (*Camellia sinensis* L.) seed shells	7.5	324.7	(Gao et al., 2013)
Hydrous manganese oxide-coated alum	4-6	7.09	(Teng et al., 2009)
Carbonized watermelon (*Citrullus lanatus*) rind prepared *via* one-step liquid phase H_2SO_4 activation	3-9	200	(Jawad et al., 2019)
Native watermelon rind	7	239.7	(Lakshmipathy & Sarada, 2016)
Banana peel biochar/iron oxide composite	6.1	862	(Zhang et al., 2020)
Wodyetia bifurcata biochar	-	149.3	(Santos et al., 2019)
8PWMR	Adsorption Unaffected by pH of solution	238.09	This study

The comparison of adsorption capacity of various adsorbents reported in literature for methylene blue removal are summarised in Table 2.10. 8PWMR was observed to be a better adsorbent than other adsorbents reported in literature due to its effectiveness over a wide pH range and high Langmuir adsorption capacity. Activated carbon from *Posidonia oceanica* (L.) dead leaves also gave comparable results (Boukmouche et al., 2014).

2.5.2.6 Adsorption kinetics and thermodynamics

To figure out adsorption mechanism pseudo-first-order, pseudo-second-order and intraparticle diffusion models were investigated (figure 2.20) and the calculated rate constants and r^2 values are tabulated in table 2.11.

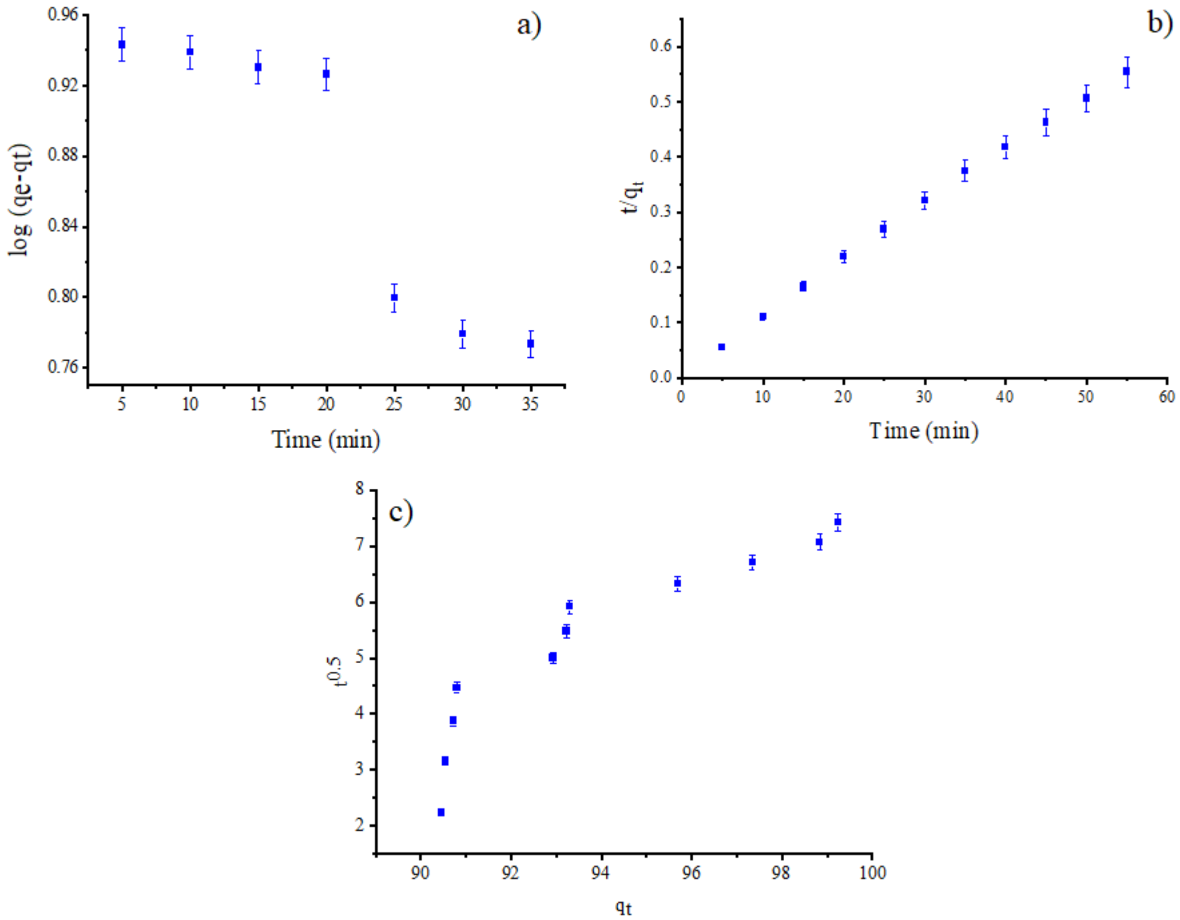

Figure 2.20 Kinetic models for methylene blue adsorption onto 8PWMR a) Pseudo first order, b) Pseudo second order, c) Intraparticle diffusion

It was observed that the adsorption data of MB by 8PWMR were best fitted with pseudo-second order model since the regression coefficient (r^2) value at 303 K was 0.99 than that of pseudo-first order that is 0.83. Moreover, the experimental q_e values were closer to the calculated q_e values of pseudo-second order model than pseudo-first order model, suggesting the reaction kinetics is of pseudo-second order. The mechanism which controls the rate of reaction is the chemical sorption say valence forces where sharing and/or exchange of electrons between adsorbent and adsorbate occurs. Due to this the kinetic data were further analysed by intraparticle diffusion model to study the mechanism of diffusion. The study of the intraparticle diffusion model gave r^2 value 0.97 and the plot between sorbate concentration and square root of time was linear suggesting that the adsorption process could be controlled by intraparticle diffusion.

Table 2.9 Kinetic parameters

Kinetic parameters			
q_t (exp): 4.675mg/g	**q_t**	**K**	**r^2**
Pseudo First order	10.16	0.0002	0.83
Pseudo Second order	101.01	0.016	0.99
Intraparticle diffusion	2.99	0.099	0.97

2.5.2.7 Reuse of adsorbent

To study the reusability of adsorbent, the desorption was first performed using 0.1M NaOH solution. After the desorption the adsorbent was dried and reused for the adsorption process. The % uptake of methylene blue was found to be 99,98%, 98.85%, 96.24% and 95.68% for the 1st 2nd 3rd and 4th cycle of batch operations respectively (figure 2.22). The result shows the good sustainability of adsorbent for commercial or industrial purposes.

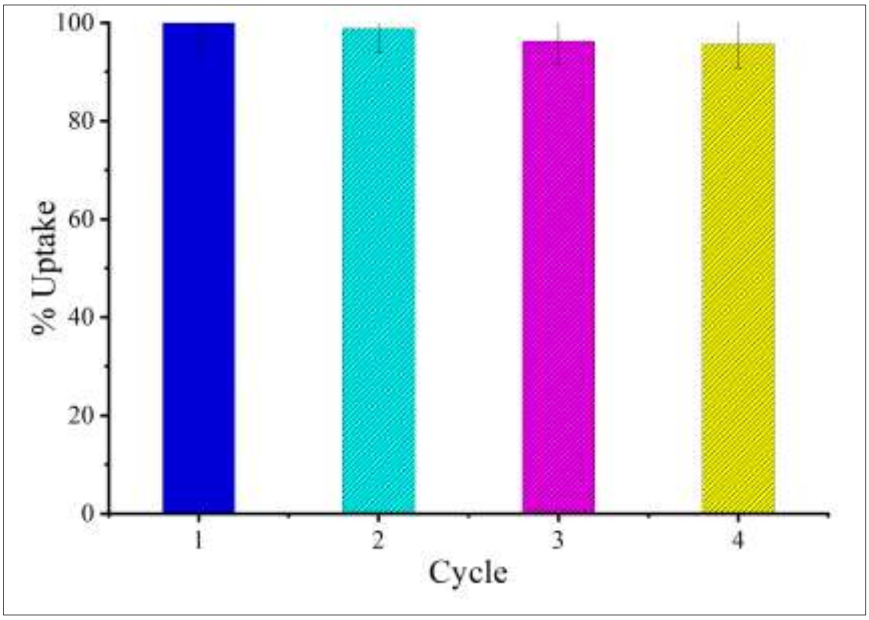

Figure 2.21 % uptake of methylene blue after consecutive 1st 2nd 3rd and 4th cycles

2.5.3 Characterization of 8PWMR after adsorption of MB

Scanning electron microscopy and Energy dispersive X-ray analysis:

The EDAX analysis of 8PWMRMB are shown in the insets of figure 2.23. The rise in S, C and O content in 8PWMRMB could be attributed to the uptake of methylene blue.

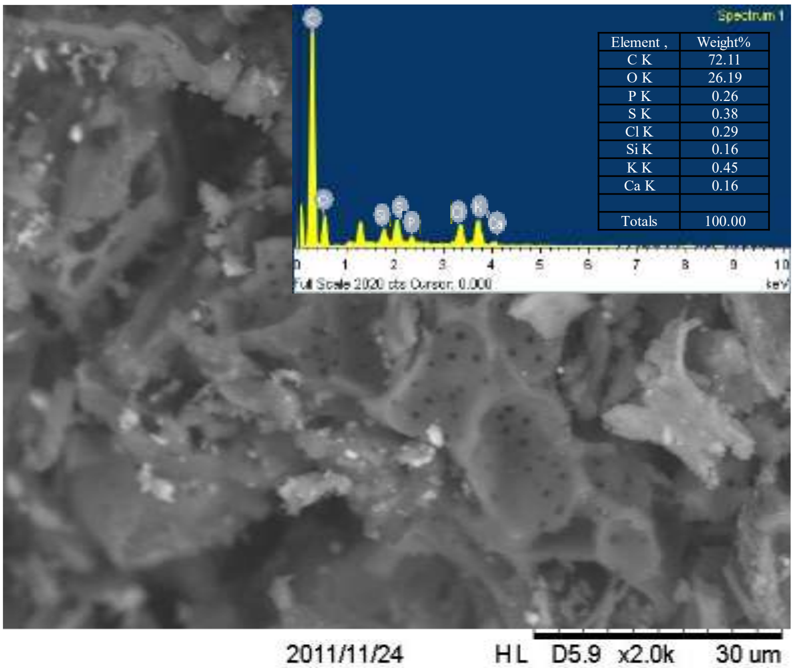

Figure 2.22 SEM-EDAX analysis of 8PWMRMB

FTIR spectral analysis

Figure 2.24 shows the IR spectra of the 8PWMRMB. The band at 3699 cm^{-1} was ascribed to -OH stretching vibration, while the peak at 2900 cm^{-1} was attributed to C-H stretching vibration. Carboxyl C=O stretching vibrations and C=C peaks were identified at 1549 cm^{-1}; the peak at 1047 cm^{-1} was ascribed to the C-OH stretching vibration (Ying et al., 2021).

There is a shift of peaks such as 2372 (in 8PWMR) from 2332 cm^{-1} (in 8PWMRMB) (O-H stretch of the carboxylic group), and 1549 cm^{-1} (aromatic), indicating that these functional groups may have interacted with the MB (Suhaimi et al., 2022).

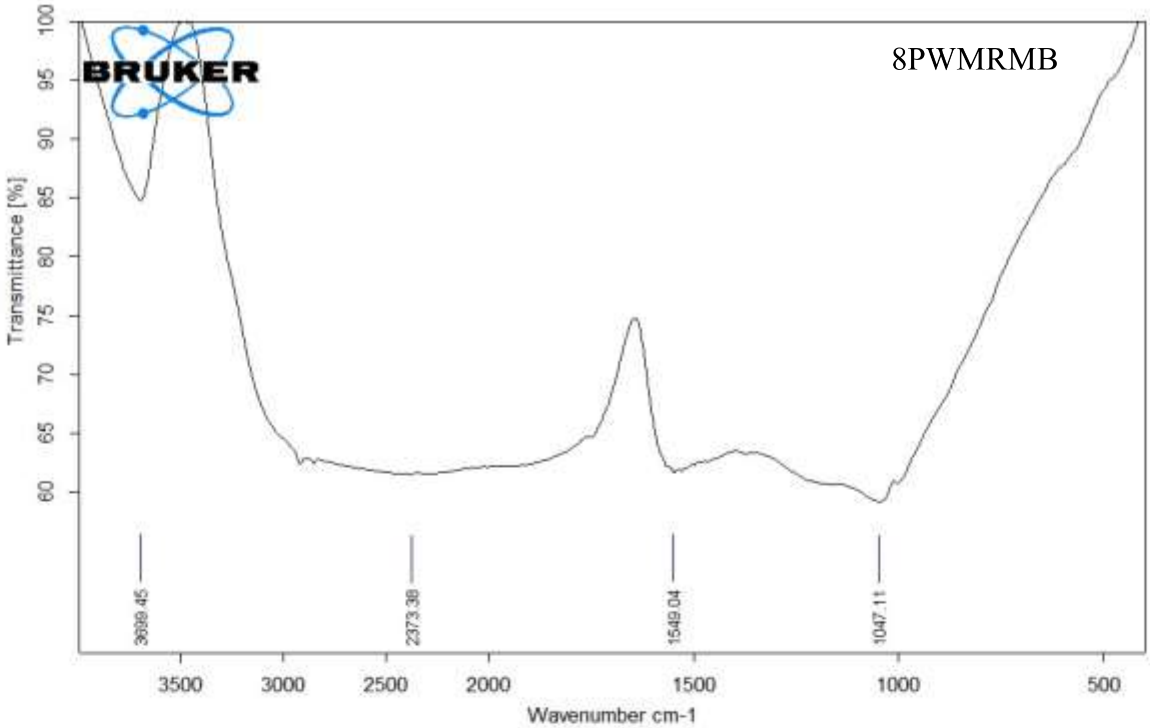

Figure 2. 23 IR spectra of 8PWMRB

2.5.4 Conclusions

In this study biochar derived from water melon rind, 8PWMR was used to remove methylene blue from aqueous solutions. Batch experiments showed that the adsorbent works very good in whole pH range and the maximum adsorption occurs in initial 30 mins with 0.05 g dose for MB. The maximum adsorption capacity was found to be 238.09 mg/g for MB. The experimental isotherm fitted well to the Freundlich isotherm. The adsorption kinetic data successfully followed the pseudo second order kinetic model. The negative values of free energy and enthalpy indicated the spontaneous and exothermic nature of the adsorption process. The performance of the adsorbent for synthetic effluent was demonstrated. The mechanism of dye adsorption on 8PWMR is governed mainly by electrostatic, hydrogen bonding and π-π stacking interactions. Finally, it can be concluded that the 8PWMR is an efficient, low-cost and sustainable adsorbent for removal cationic dye species such as methylene blue from aqueous solutions and even in industrial effluent.

2.6 References

Altenor, S., Carene, B., Emmanuel, E., Lambert, J., Ehrhardt, J. J., & Gaspard, S. (2009). Adsorption studies of methylene blue and phenol onto vetiver roots activated carbon prepared by chemical activation. *Journal of Hazardous Materials*, *165*(1–3), 1029–1039. https://doi.org/10.1016/j.jhazmat.2008.10.133

Armbruster, M. H., & Austin, J. B. (1938). The Adsorption of Gases on Plane Surfaces of Mica. *Journal of the American Chemical Society*, *60*(2), 467–475. https://doi.org/10.1021/ja01269a066

Attia, A. A., Girgis, B. S., & Fathy, N. A. (2008). Removal of methylene blue by carbons derived from peach stones by H_3PO_4 activation: Batch and column studies. *Dyes and Pigments*, *76*(1), 282–289. https://doi.org/10.1016/j.dyepig.2006.08.039

Başar, C. A. (2006). Applicability of the various adsorption models of three dyes adsorption onto activated carbon prepared waste apricot. *Journal of Hazardous Materials*, *135*(1–3), 232–241. https://doi.org/10.1016/j.jhazmat.2005.11.055

Bell, D. (2011). Daniel Bell. *New York*, 12–14. https://doi.org/10.4324/9780203129357

Bhatnagar, A., Kumar, E., & Sillanpää, M. (2011). Fluoride removal from water by adsorption-A review. In *Chemical Engineering Journal*. https://doi.org/10.1016/j.cej.2011.05.028

Bokhari, A., Chuah, L. F., Yusup, S., Klemeš, J. J., Akbar, M. M., & Kamil, R. N. M. (2016). Cleaner production of rubber seed oil methyl ester using a hydrodynamic cavitation: Optimisation and parametric study. *Journal of Cleaner Production*. https://doi.org/10.1016/j.jclepro.2016.04.091

Boukmouche, N., Azzouz, N., Bouchama, L., Chopart, J. P., & Bouznit, Y. (2014). Activated carbon derived from marine Posidonia Oceanica for electric energy storage. *Arabian Journal of Chemistry*, *7*(3), 347–354. https://doi.org/https://doi.org/10.1016/j.arabjc.2012.12.010

Braik, S., Amor, T. Ben, Michelin, L., Rigolet, S., Bonne, M., Lebeau, B., & Hafiane, A. (2022). Natural water defluoridation by adsorption on Laponite clay. *Water Science and Technology*, *85*(6), 1701–1719. https://doi.org/10.2166/wst.2022.091

Brewer, C. E., Schmidt-Rohr, K., Satrio, J. A., & Brown, R. C. (2009). Characterization of biochar from fast pyrolysis and gasification systems. *Environmental Progress and Sustainable Energy*, *28*(3), 386–396. https://doi.org/10.1002/ep.10378

Budrat, P., & Shotipruk, A. (2009). Enhanced recovery of phenolic compounds from bitter melon (*Momordica charantia*) by subcritical water extraction. *Separation and Purification Technology*, *66*(1), 125–129. https://doi.org/10.1016/j.seppur.2008.11.014

Budyanto, S., Kuo, Y.-L., & Liu, J. C. (2015). Adsorption and precipitation of fluoride on calcite nanoparticles: A spectroscopic study. *Separation and Purification Technology*, *150*, 325–331. https://doi.org/10.1016/j.seppur.2015.07.016

Cabeza, A., Sobrón, F., Yedro, F. M., & García-Serna, J. (2015). Autocatalytic kinetic model for thermogravimetric analysis and composition estimation of biomass and polymeric fractions. *Fuel*, *148*, 212–225. https://doi.org/10.1016/j.fuel.2015.01.048

Dari, B., Nair, V. D., Harris, W. G., Nair, P. K. R., Sollenberger, L., & Mylavarapu, R. (2016). Relative influence of soil- vs. biochar properties on soil phosphorus retention. *Geoderma*, *280*, 82–87. https://doi.org/10.1016/j.geoderma.2016.06.018

Deng, H., Yang, L., Tao, G., & Dai, J. (2009). Preparation and characterization of activated carbon from cotton stalk by microwave assisted chemical activation-Application in methylene blue adsorption from aqueous solution. *Journal of Hazardous Materials*, *166*(2–3), 1514–1521. https://doi.org/10.1016/j.jhazmat.2008.12.080

Dhawane, S. H., Khan, A. A., Singh, K., Tripathi, A., Hasda, R., & Halder, G. (2018). Insight into Optimization, isotherm, kinetics, and thermodynamics of fluoride adsorption onto activated alumina. *Environmental Progress and Sustainable Energy*. https://doi.org/10.1002/ep.12814

dos Santos, K. J. L., dos Santos, G. E. de S., de Sá, Í. M. G. L., Ide, A. H., Duarte, J. L. da S., de Carvalho, S. H. V., Soletti, J. I., & Meili, L. (2019). Wodyetia bifurcata biochar for methylene blue removal from aqueous matrix. *Bioresource Technology*, *293*, 122093. https://doi.org/10.1016/j.biortech.2019.122093

Dural, M. U., Cavas, L., Papageorgiou, S. K., & Katsaros, F. K. (2011). Methylene blue adsorption on activated carbon prepared from Posidonia oceanica (L.) dead leaves: Kinetics and equilibrium studies. *Chemical Engineering Journal*, *168*(1), 77–85. https://doi.org/10.1016/j.cej.2010.12.038

El Qada, E. N., Allen, S. J., & Walker, G. M. (2006). Adsorption of Methylene Blue onto activated carbon produced from steam activated bituminous coal: A study of equilibrium adsorption isotherm. *Chemical Engineering Journal*, *124*(1–3), 103–110. https://doi.org/10.1016/j.cej.2006.08.015

Foo, K. Y., & Hameed, B. H. (2011). Preparation of activated carbon from date stones by microwave induced chemical activation: Application for methylene blue adsorption.

Chemical Engineering Journal, *170*(1), 338–341. https://doi.org/10.1016/j.cej.2011.02.068

Fuente, E., Menéndez, J. A., Díez, M. A., Suárez, D., & Montes-Morán, M. A. (2003). Infrared Spectroscopy of Carbon Materials: A Quantum Chemical Study of Model Compounds. *The Journal of Physical Chemistry B*, *107*(26), 6350–6359. https://doi.org/10.1021/jp027482g

Gao, J., Qin, Y., Zhou, T., Cao, D., Xu, P., Hochstetter, D., & Wang, Y. (2013). Adsorption of methylene blue onto activated carbon produced from tea (Camellia sinensis L.) seed shells: kinetics, equilibrium, and thermodynamics studies. *Journal of Zhejiang University SCIENCE B*, *14*(7), 650–658. https://doi.org/10.1631/jzus.B12a0225

Geçgel, Ü., Özcan, G., & Gürpnar, G. Ç. (2013). Removal of methylene blue from aqueous solution by activated carbon prepared from pea shells (Pisum sativum). *Journal of Chemistry*. https://doi.org/10.1155/2013/614083

Gerçel, Ö., Özcan, A., Özcan, A. S., & Gerçel, H. F. (2007). Preparation of activated carbon from a renewable bio-plant of Euphorbia rigida by H_2SO_4 activation and its adsorption behavior in aqueous solutions. *Applied Surface Science*, *253*(11), 4843–4852. https://doi.org/10.1016/j.apsusc.2006.10.053

Ho, Y. S., & McKay, G. (1998). Sorption of dye from aqueous solution by peat. *Chemical Engineering Journal*, *70*(2), 115–124. https://doi.org/10.1016/S1385-8947(98)00076-X

Horax, R., Hettiarachchy, N., & Islam, S. (2005). Total Phenolic Contents and Phenolic Acid Constituents in 4 Varieties of Bitter Melons (Momordica charantia) and Antioxidant Activities of Their Extracts. *Journal of Food Science*, *70*(4), 275–280. https://doi.org/10.1111/j.1365-2621.2005.tb07173.x

Jawad, A. H., Razuan, R., Appaturi, J. N., & Wilson, L. D. (2019). Adsorption and mechanism study for methylene blue dye removal with carbonized watermelon (Citrullus lanatus)rind prepared via one-step liquid phase H_2SO_4 activation. *Surfaces and Interfaces*, *16*, 76–84. https://doi.org/10.1016/j.surfin.2019.04.012

Jin, X., Xi, F., Lv, D., Wu, Q., & Lin, X. (2011a). The effect of the chitosan membrane properties on the enzyme adsorption and performance for the construction of horseradish peroxidase biosensors. *Carbohydrate Polymers*, *85*(4), 786–791.

https://doi.org/10.1016/j.carbpol.2011.03.048

Jin, X., Xi, F., Lv, D., Wu, Q., & Lin, X. (2011b). The effect of the chitosan membrane properties on the enzyme adsorption and performance for the construction of horseradish peroxidase biosensors. *Carbohydrate Polymers*, *85*(4), 786–791. https://doi.org/http://dx.doi.org/10.1016/j.carbpol.2011.03.048

Jin, Z., Wang, X., Sun, Y., Ai, Y., & Wang, X. (2015). Adsorption of 4-n-Nonylphenol and Bisphenol-A on Magnetic Reduced Graphene Oxides: A Combined Experimental and Theoretical Studies. *Environmental Science & Technology*, *49*(15), 9168–9175. https://doi.org/10.1021/acs.est.5b02022

Khan, T. A., Chaudhry, S. A., & Ali, I. (2015). Equilibrium uptake, isotherm and kinetic studies of Cd(II) adsorption onto iron oxide activated red mud from aqueous solution. *Journal of Molecular Liquids*, *202*, 165–175. https://doi.org/10.1016/j.molliq.2014.12.021

Kishore, M. (2011). Preparation and development of adsorbent carbon from acacia farnesiana for defluoridation. *International Journal of Plant, Animal and Environmental Sciences*, *3*, 209–223.

Kumar, H., Patel, M., & Mohan, D. (2019). Simplified Batch and Fixed-Bed Design System for Efficient and Sustainable Fluoride Removal from Water Using Slow Pyrolyzed Okra Stem and Black Gram Straw Biochars. *ACS Omega*. https://doi.org/10.1021/acsomega.9b00877

Kumar, P. S., Ramalingam, S., & Sathishkumar, K. (2011). Removal of methylene blue dye from aqueous solution by activated carbon prepared from cashew nut shell as a new low-cost adsorbent. *Korean Journal of Chemical Engineering*, *28*(1), 149–155. https://doi.org/10.1007/s11814-010-0342-0

Kushwaha, S., Sreelatha, G., & Padmaja, P. (2013). Physical and chemical modified forms of palm shell: Preparation, characterization and preliminary assessment as adsorbents. *Journal of Porous Materials*, *20*(1), 21–36. https://doi.org/10.1007/s10934-012-9571-4

Lakshmipathy, R., & Sarada, N. C. (2016). Methylene blue adsorption onto native watermelon rind: batch and fixed bed column studies. *Desalination and Water Treatment*, *57*(23), 10632–10645. https://doi.org/10.1080/19443994.2015.1040462

Lee, Y., Eum, P. R. B., Ryu, C., Park, Y. K., Jung, J. H., & Hyun, S. (2013). Characteristics of biochar produced from slow pyrolysis of Geodae-Uksae 1. *Bioresource Technology*, *130*, 345–350. https://doi.org/10.1016/j.biortech.2012.12.012

Lei, W., Li, T., Lv, N., Liu, H., Zhang, Y., & Xi, B. (2019). Study on adsorption of lead by biochar prepared from sludge of municipal wastewater treatment plant. *IOP Conference Series: Materials Science and Engineering*, *479*, 12007. https://doi.org/10.1088/1757-899X/479/1/012007

Li, K., Zheng, Z., Huang, X., Zhao, G., Feng, J., & Zhang, J. (2009). Equilibrium, kinetic and thermodynamic studies on the adsorption of 2-nitroaniline onto activated carbon prepared from cotton stalk fibre. *Journal of Hazardous Materials, 166*(1), 213–220. https://doi.org/https://doi.org/10.1016/j.jhazmat.2008.11.007

Liu, S., Peng, S., Zhang, B., Xue, B., Yang, Z., Wang, S., & Xu, G. (2022). Effects of biochar pyrolysis temperature on thermal properties of polyethylene glycol/biochar composites as shape-stable biocomposite phase change materials. *RSC Adv.*, *12*(16), 9587–9598. https://doi.org/10.1039/D1RA09167K

Mimmo, T., Panzacchi, P., Baratieri, M., Davies, C. A., & Tonon, G. (2014). Effect of pyrolysis temperature on miscanthus (Miscanthus × giganteus) biochar physical, chemical and functional properties. *Biomass and Bioenergy*, *62*, 149–157. https://doi.org/10.1016/j.biombioe.2014.01.004

Misran, E., Bani, O., Situmeang, E. M., & Purba, A. S. (2018). Removal efficiency of methylene blue using activated carbon from waste banana stem: Study on pH influence. *IOP Conference Series: Earth and Environmental Science*, *122*(1). https://doi.org/10.1088/1755-1315/122/1/012085

Mohan, D., Kumar, S., & Srivastava, A. (2014). Fluoride removal from ground water using magnetic and nonmagnetic corn stover biochars. *Ecological Engineering*, *73*, 798–808. https://doi.org/10.1016/j.ecoleng.2014.08.017

Mohan, D., Sharma, R., Singh, V. K., Steele, P., & Pittman, C. U. (2012a). Fluoride removal from water using bio-char, a green waste, low-cost adsorbent: Equilibrium uptake and sorption dynamics modeling. *Industrial and Engineering Chemistry Research*, *51*(2), 900–914. https://doi.org/10.1021/ie202189v

Mohan, D., Sharma, R., Singh, V. K., Steele, P., & Pittman, C. U. (2012b). Fluoride Removal from Water using Bio-Char, a Green Waste, Low-Cost Adsorbent: Equilibrium Uptake and Sorption Dynamics Modeling. *Industrial & Engineering Chemistry Research*, *51*(2), 900–914. https://doi.org/10.1021/ie202189v

Morterra, C., & Low, M. J. D. (1982). The Nature of the 1600 cm−1 Band of Carbons. *Spectroscopy Letters*, *15*(9), 689–697. https://doi.org/10.1080/00387018208068024

Mukherjee, S., & Halder, G. (2016). Assessment of fluoride uptake performance of raw biomass and activated biochar of Colocasia esculenta stem: Optimization through response surface methodology. *Environmental Progress & Sustainable Energy*, *35*(5), 1305–1316. https://doi.org/10.1002/ep.12346

N., G., D., S., K.B., C. S., & S., A. (2012). Removal of fluoride from water and waste water by using low cost adsorbents. *International Journal of PharmTech Research*, *4*(4), 1646–1653. http://www.embase.com/search/results?subaction=viewrecord&from=export&id=L366053114%5Cnhttp://www.sphinxsai.com/2012/oct-dec/chempdf/CT=58(1646-1653)OD12.pdf%5Cnhttp://wx7cf7zp2h.search.serialssolutions.com?sid=EMBASE&issn=09744304&id=doi:&atitle=Removal+of

Odewunmi, N. A., Umoren, S. A., Gasem, Z. M., Ganiyu, S. A., & Muhammad, Q. (2015). l-Citrulline: An active corrosion inhibitor component of watermelon rind extract for mild steel in HCl medium. *Journal of the Taiwan Institute of Chemical Engineers*, *51*(February), 177–185. https://doi.org/10.1016/j.jtice.2015.01.012

Pasieczna-Patkowska, S., & Madej, J. (2018). Comparison of photoacoustic, diffuse reflectance, attenuated total reflectance and transmission infrared spectroscopy for the study of biochars. *Polish Journal of Chemical Technology*, *20*, 75–83. https://doi.org/10.2478/pjct-2018-0057

Patel, G., Pal, U., & Menon, S. (2009). Removal of Fluoride from Aqueous Solution by CaO Nanoparticles. *Separation Science and Technology*, *44*(12), 2806–2826. https://doi.org/10.1080/01496390903014425

Pathania, D., Sharma, S., & Singh, P. (2017). Removal of methylene blue by adsorption onto activated carbon developed from Ficus carica bast. *Arabian Journal of Chemistry*, *10*, S1445–S1451. https://doi.org/10.1016/j.arabjc.2013.04.021

Petkowicz, C., Vriesmann, L., & Williams, P. A. (2016). Pectins from food waste: Extraction, characterization and properties of watermelon rind pectin. *Food Hydrocolloids*, *65*. https://doi.org/10.1016/j.foodhyd.2016.10.040

Rehrah, D., Reddy, M. R., Novak, J. M., Bansode, R. R., Schimmel, K. A., Yu, J., Watts, D. W., & Ahmedna, M. (2014). Production and characterization of biochars from agricultural by-products for use in soil quality enhancement. *Journal of Analytical and Applied Pyrolysis*, *108*, 301–309. https://doi.org/10.1016/j.jaap.2014.03.008

Sadhu, M., Bhattacharya, P., Vithanage, M., & Padmaja Sudhakar, P. (2022). Adsorptive removal of fluoride using biochar – A potential application in drinking water treatment. *Separation and Purification Technology*, *278*(February 2021), 119106. https://doi.org/10.1016/j.seppur.2021.119106

Sahoo, K., Kumar, A., & Chakraborty, J. P. (2021). A comparative study on valuable products: bio-oil, biochar, non-condensable gases from pyrolysis of agricultural residues. *Journal of Material Cycles and Waste Management*, *23*(1), 186–204. https://doi.org/10.1007/s10163-020-01114-2

Schwanninger, M., Rodrigues, J. C., Pereira, H., & Hinterstoisser, B. (2004). Effects of short-time vibratory ball milling on the shape of FT-IR spectra of wood and cellulose. *Vibrational Spectroscopy*, *36*(1), 23–40. https://doi.org/10.1016/j.vibspec.2004.02.003

Singh, T. (2015). Removal of fluoride using treated banana peel in batch reactor: kinetics and equilibrium studies. *World journal of pharmacy and pharmaceutical sciences*, *04*, 693–704.

Suhaimi, N., Kooh, M. R. R., Lim, C. M., Chou Chao, C.-T., Chou Chau, Y.-F., Mahadi, A. H., Chiang, H.-P., Haji Hassan, N. H., & Thotagamuge, R. (2022). The Use of *Gigantochloa* Bamboo-Derived Biochar for the Removal of Methylene Blue from Aqueous Solution. *Adsorption Science & Technology*, *2022*, 8245797. https://doi.org/10.1155/2022/8245797

Sujana, M. G., & Anand, S. (2011). Fluoride removal studies from contaminated ground water by using bauxite. *Desalination*. https://doi.org/10.1016/j.desal.2010.09.030

Tan, T. L., Krusnamurthy, P. A., Nakajima, H., & Rashid, S. A. (2020). Adsorptive{,} kinetics and regeneration studies of fluoride removal from water using zirconium-based metal organic frameworks. *RSC Adv.*, *10*(32), 18740–18752. https://doi.org/10.1039/D0RA01268H

Tanaka, D. A. P., Kerketta, S., Tanco, M. A. L., Yokoyama, T., & Suzuki, T. M. (2002). Adsorption of fluoride ion on the zirconium(IV) complexes of the chelating resins functionalized with amine-N-acetate ligands. *Separation Science and Technology*, *37*(4), 877–894. https://doi.org/10.1081/SS-120002221

Tarazona-Díaz, M. P., Viegas, J., Moldao-Martins, M., & Aguayo, E. (2011). Bioactive compounds from flesh and by-product of fresh-cut watermelon cultivars. *Journal of the Science of Food and Agriculture*, *91*(5), 805–812. https://doi.org/10.1002/jsfa.4250

Teng, S.-X., Wang, S.-G., Gong, W.-X., Liu, X.-W., & Gao, B.-Y. (2009). Removal of fluoride by hydrous manganese oxide-coated alumina: Performance and mechanism [JOUR]. *Journal of Hazardous Materials*, *168*(2–3), 1004–1011. https://doi.org/http://doi.org/10.1016/j.jhazmat.2009.02.133

Thue, P. S., Sophia, A. C., Lima, E. C., Wamba, A. G. N., de Alencar, W. S., dos Reis, G. S., Rodembusch, F. S., & Dias, S. L. P. (2018). Synthesis and characterization of a novel organic-inorganic hybrid clay adsorbent for the removal of acid red 1 and acid green 25 from aqueous solutions. *Journal of Cleaner Production*, *171*, 30–44. https://doi.org/10.1016/j.jclepro.2017.09.278

Wang, H., Lin, K., Hou, Z., Richardson, B., & Gan, J. (2010). Sorption of the herbicide terbuthylazine in two New Zealand forest soils amended with biosolids and biochars. *Journal of Soils and Sediments*, *10*(2), 283–289. https://doi.org/10.1007/s11368-009-0111-z

Wu, W., Yang, M., Feng, Q., McGrouther, K., Wang, H., Lu, H., & Chen, Y. (2012). Chemical characterization of rice straw-derived biochar for soil amendment. *Biomass and Bioenergy*, *47*, 268–276. https://doi.org/10.1016/j.biombioe.2012.09.034

Yang, X. B., Ying, G. G., Peng, P. A., Wang, L., Zhao, J. L., Zhang, L. J., Yuan, P., & He, H. P. (2010). Influence of biochars on plant uptake and dissipation of two pesticides in an agricultural soil. *Journal of Agricultural and Food Chemistry*, *58*(13), 7915–7921. https://doi.org/10.1021/jf1011352

Ying, Z., Chen, X., Li, H., Liu, X., Zhang, C., Zhang, J., & Yi, G. (2021). Efficient Adsorption of Methylene Blue by Porous Biochar Derived from Soybean Dreg Using a One-Pot Synthesis Method. *Molecules (Basel, Switzerland)*, *26*(3). https://doi.org/10.3390/molecules26030661

Zhang, P., O'Connor, D., Wang, Y., Jiang, L., Xia, T., Wang, L., Tsang, D. C. W., Ok, Y. S., & Hou, D. (2020). A green biochar/iron oxide composite for methylene blue removal. *Journal of Hazardous Materials*, *384*, 121286. https://doi.org/https://doi.org/10.1016/j.jhazmat.2019.121286

Zhao, J., Shen, X.-J., Domene, X., Alcañiz, J.-M., Liao, X., & Palet, C. (2019). Comparison of biochars derived from different types of feedstock and their potential for heavy metal removal in multiple-metal solutions. *Scientific Reports*, *9*(1), 9869. https://doi.org/10.1038/s41598-019-46234-4

Zhou, J., Liu, Y., Han, Y., Jing, F., & Chen, J. (2019). Bone-derived biochar and magnetic biochar for effective removal of fluoride in groundwater: Effects of synthesis method and coexisting chromium. *Water Environment Research*. https://doi.org/10.1002/wer.1068